

The Himalayan Frontal Thrust of India is not blind

Senthil Kumar¹, Steven G. Wesnousky¹, Thomas K. Rockwell², Richard W. Briggs¹,
Vikram C. Thakur³, R. Jayangondaperumal³

¹Center for Neotectonic Studies, University of Nevada, Reno NV 89577, USA

²Department of Geological Sciences, San Diego State University, San Diego CA 92182, USA

²Wadia Institute of Himalayan Geology, Dehra Dun, UA 248 001, INDIA

ABSTRACT

We report evidence of surface rupturing earthquakes at Chandigarh, Kala Amb, Rampur Ganda, Dehradun, Lal Dhang, and Ramnagar covering a distance of ~400 km along strike of the Himalayan Frontal Thrust (HFT) of India. Trench exposures across the HFT and radiocarbon ages place limits on the timing of the last surface rupture at each site, but Dehradun, during the last ~600 years: Chandigarh (1404 – ~1600 A.D.), Kala Amb (1424 – 1950 A.D.), Rampur Ganda (1222 – 1422 A.D.), Lal Dhang (1282 – 1632 A.D.), and Ramnagar (1263 – 1433 A.D.). The overlapping ages allow the interpretation that all sites ruptured simultaneously at about 1413 ± 9 A.D. (or, between 1404 – 1422 A.D.). The interpretation is consistent with the large coseismic displacements observable at Rampur Ganda, Lal Dhang, and Ramnagar. At these sites, trench exposures and vertical separations of ~9 – 13 m are interpreted to indicate ~18 – 26 m of coseismic slip during the last surface rupture earthquake, assuming an average fault dip of 30°. The sites at Chandigarh and Kala Amb may also preserve evidence of a penultimate earthquake. Long-term displacement on the HFT has resulted in the occurrence of uplifted and truncated fluvial strath terraces along canyons of the Ghaggar, Markanda, Shajahanpur, Kosi and Nandaur Rivers. Minimum vertical uplift rates of the terraces are estimated at 5 to 11 mm/yr by dividing the elevation of

the terraces by the maximum radiocarbon age of the terrace abandonment. Dividing observed single event vertical displacements at Rampur Ganda, Lal Dhang, and Ramnagar by the estimated longer-term uplift rates indicates 1 – 2 thousand years would be needed to accumulate the slip released during the most recent surface rupture earthquake. Assuming an average dip of 30° for the HFT, the long-term uplift rates of 5 to 11 mm/yr equates to fault slip rates of 10 to 22 mm/yr and shortening rates of 9 to 19 mm/yr. Given that we observe clear evidence of surface rupture earthquakes and its long-term geologic expression in progressive and continued offset of fluvial terraces, the question arises as to why surface rupture has not been recorded in the well-documented major historical events of the 1905 Kangra earthquake, 1934 Bihar-Nepal earthquake, and 1950 Assam earthquake that occurred during the last century. We suggest on the basis of size and possible synchronicity of the most recent displacement recorded between 1404 and 1422 A.D. (or, 1413 ± 9 A.D.) that the earthquake recorded in the trenches is larger than historical earthquakes and indicate a potential for sections of the HFT to rupture simultaneously along lengths of the HFT greater than the ~400 km we have studied.

INTRODUCTION

The ongoing collision of India into Eurasia has resulted in three major earthquakes along the Himalayan front during the past ~100 years (Seeber and Armbruster, 1981) (**Figure 1A**). From east to west, the sequence includes the 1905 Kangra earthquake (M_s ~7.8), the 1934 Bihar-Nepal earthquake ($M = 7.7 \pm 0.2$), and the 1950 Assam earthquake ($M_w \sim 8.6$) (Pandey and Molnar, 1988; Ambraseys and Bilham, 2000; Bilham, 2001).

Although none of the earthquakes are reported to have produced primary surface rupture (Seeber and Armbruster, 1981), it has generally been assumed on the basis of isoseismals and location that the earthquakes are the result of slip on the Himalayan Frontal Thrust (HFT). Lack of primary surface rupture during the major historical earthquakes has led previous workers to attribute their occurrence to a blind thrust, whereby strain release is expressed as anticline growth rather than primary surface rupture or coseismic surface rupture (Stein and Yeats, 1989; Yeats et al., 1992; Yeats and Thakur, 1998). In this paper, we describe the late Quaternary expression of the HFT at seven sites and demonstrate that the HFT is not blind but, rather, an emergent fault system. We then discuss the mechanical implications that arise if the major historical earthquakes along the HFT have been the result of slip on the HFT but have not produced coseismic surface rupture. Finally, we discuss observations that suggest the HFT has and will produce earthquakes of size greater than those observed historically, perhaps as large as the greatest thrust earthquakes observed along the major convergent oceanic plate boundaries.

REGIONAL TECTONICS

The Himalayan mountain belt formed as a result of the collision of India into Eurasia (**Figure 1A**) and has accommodated ~2000-3000 km of convergence along the ~2500 km length of plate boundary since the Eocene (Molnar and Tapponnier, 1977). The collision has produced three major crustal-scale south verging thrust faults that strike the length of the Himalayan arc (**Figure 1A**). The northernmost is the structurally highest and oldest Main Central Thrust (MCT) system, which dips 30° to 45° northward and marks the contact

between the High Himalaya and the Lesser Himalaya (Gansser, 1964). The age of the youngest deformation in the MCT shear zone is unknown (Hodges, 2000). Seeber and Gornitz (1983) suggested that at least some segments of the MCT might still be active based on a general correlation of the MCT trace with distinctive knickpoints in the gradients of antecedent rivers that drain the southern flank of the Himalaya. However, the MCT has not been observed to cut Quaternary deposits and is generally considered inactive (Nakata, 1989). South of the MCT, the south verging Main Boundary Thrust (MBT) forms a series of north dipping thrust faults that mark the contact between the predominantly pre-Tertiary Lesser Himalayan sediments and the Tertiary and Quaternary sub-Himalayan sediments. The MBT is clearly expressed as a fault in bedrock along nearly its entire length, and in places transports pre-Tertiary to Quaternary Lesser Himalayan and sub-Himalayan sediments over younger Quaternary deposits (Nakata, 1972; Nakata, 1989; Valdiya, 1992). The MBT along the majority of the arc is expressed by south facing scarps and is locally expressed by north facing scarps (Nakata, 1989). The southernmost of the three thrusts, and focus of this paper, is the Himalayan Frontal Thrust (HFT), which marks the northern limit of the exposed Indian Plate and displaces Tertiary and Quaternary sediments of the Siwalik Group (<0.5(?)–18 Ma) over the Indo-Gangetic plain along its length (Nakata, 1972). The HFT is generally marked by the contact of the bedrock Siwalik Group and Quaternary alluvium. Locally, the HFT is expressed in young alluvium as relatively short and discontinuous range front scarps that cut Quaternary fluvial terraces and alluvial fans (Nakata, 1972; Nakata, 1989; Valdiya, 1992; Yeats et al., 1992; Wesnousky et al., 1999; Kumar et al., 2001). All three east-west striking south verging thrusts within the Eurasian plate (**Figure 1**) appear to merge into a common décollement, the Main Himalayan Thrust

(Seeber and Armbruster, 1981; Zhao et al., 1993; Brown et al., 1996; Nelson, 1998; Hodges, 2000) (**Figure 1A & 1B**).

Plate motion models and GPS measurements indicate that India – Eurasia convergence continues today at a rate of about 40 to 50 mm/year (Demets et al., 1994; Paul et al., 2001) (**Inset in Figure 1A**). Between about 10 and 20 mm/year of the total 40 to 50 mm/year is taken up by thrusting on the HFT (Bilham et al., 1997; Wesnousky et al., 1999; Lave and Avouac, 2000; Wang et al., 2001; Kumar et al., 2001). The remaining motion is absorbed by a combination of thrusting, crustal extension and strike-slip motion within the Eurasian plate (Armijo et al., 1986; Armijo et al., 1989; Avouac and Tapponnier, 1993) (**Inset in Figure 1A**). The major historical earthquakes are suggested to have originated beneath the Higher Himalaya north of the MCT and ruptured the entire basal décollement south of the Higher Himalaya up to the HFT (Seeber and Armbruster, 1981) (**Figure 1A and 1B**). The above interpretation of southward rupture propagation is consistent with the region of most severe shaking and damage associated with the major historical events shown in **Figure 1A**, which is generally bounded by the MCT to the north and HFT to the south (Seeber and Armbruster, 1981) (**Figure 1B**). It is this latter observation that is cited as the principle evidence that the 1905, 1934, and 1950 earthquakes are the result of slip on the HFT (Pandey and Molnar, 1988; Chander, 1989; Molnar and Pandey, 1989; Ambraseys and Bilham, 2000).

OBSERVATIONS

Boxes in **Figure 2** outline the specific sites discussed in the study, extending between Chandigarh in the west to Chor Ghalia in the east along ~400 km stretch of the Indian HFT. We present observations from six new sites together with a previously studied site at Kala Amb (**Figure 2**). For each site, we use structural, geomorphic, and paleoseismic data to highlight the characteristics of fault displacement along the HFT.

CHANDIGARH (SITE 1)

Between the longitude $76^{\circ} 45'$ and $77^{\circ} 00'$ E and near the city of Chandigarh (population ~809,000), displacement along the northeast to north dipping HFT has produced an anticline within the Siwalik Group in the hanging wall (**Site 1, Figure 2, Figure 3**). The anticlinal axis strikes NW from Pinjore Garden with dips of $\sim 10\text{-}20^{\circ}$ SW and $20\text{-}45^{\circ}$ NE on the southwest and northwest flanks of the anticline (**Figure 3**). The anticlinal axis takes a sharp southward bend near the Ghaggar River and then changes to a near easterly strike and parallels north of and close to the HFT. The Siwalik beds on the backlimb of the asymmetric south-verging anticline southeast of the Ghaggar River show northerly dips ranging between 15° and 45° and $\sim 20^{\circ}$ southward on the south limb of the fold structure (Sahni and Kahn, 1964; Nanda, 1979); **Figure 3**).

Fault scarps in Quaternary alluvium are evident along the main trace of the HFT where it cuts and uplifts fluvial terrace deposits along the perennial Ghaggar River (**Figures**

3 and 4). Five distinct and broad fluvial terrace surfaces here were first recognized by Nakata (1972, 1989) and named the Ghaggar Terrace Surface (Qt1), Kalka Terrace Surface (Qt2), Pinjore Terrace Surface (Qt3), Lower River Terrace Surface (Qt4) and Modern River Terrace Surface (Qt5) (**Figure 4**). Each is truncated by the HFT with the exception of the youngest Qt5 terrace surface. The Ghaggar Terrace (Qt1), sits about 70 m above the present river grade, is deeply dissected, and is capped by 12 m thick fluvial deposits of weathered and sub-rounded cobble gravel (Nakata, 1972). The Kalka Terrace (Qt2) is preserved as a broad and flat surface that is ~60 m above the present river grade. Fluvial strath deposits on the Kalka surface consist of boulders and cobbles capped by ~10 m thick overbank deposits. The strath gravels sit unconformably on top of the Siwalik bedrock strath surface (Nakata, 1972). The Pinjore surface (Qt3) sits approximately 25 m above the river grade and is preserved as a wide, flat terrace to the southwest of the Kalka Terrace (Qt2). The Pinjore surface (Qt3) is capped by thick fluvial deposits up to 12 m thick consisting of boulder gravel and overlain by fine-grained overbank deposits, all sitting unconformably on the Siwalik bedrock (Nakata, 1972). The Lower River Terrace (Qt4) deposits form a broad and flat surface and the fluvial strath deposits are typically 12 m in thickness, with the terrace surface and strath bedrock contact at about 20 m and 32 m above the current stream grade, respectively. The Modern River Terrace Surface (Qt5) sits about 15 m above present river grade (**Figure 4**) and is capped by a thin veneer of fluvial gravels and overbank deposits which rest unconformably on the northeast dipping Siwalik bedrock and are not cut by the HFT. A radiometric date obtained on charcoal sample recovered within the fluvial strath deposit and below the active soil provided a post-1950 A.D. age (Sample JHA-02, **Table 1**).

The asymmetry of terrace preservation reflects possible lateral migration of the Ghaggar River during formation. The truncation of the Qt2, Qt3, and Qt4 surfaces by the HFT suggests they have been abandoned and preserved primarily as a result of tectonic uplift. The incision of the modern Qt5 terrace by the Ghaggar River, which ranges from 15 m at Gunthala to 8 m to the south of the HFT, is most likely attributable to human activity within the drainage basin (**Figure 4**). Radiocarbon dates of detrital charcoal collected from Qt4 deposits on both sides of the river place a limit on the age of the Qt4 surface. Two fragments of charcoal collected from a natural exposure of a fine-grained overbank deposit 3.3-3.5 m below the Lower River Terrace surface (Qt4) near the village of Gunthala on the southeastern margin of the Ghaggar River (sample GAG-03 and GAG-05, **Table 1, Figure 4**) yielded ages ranging between 1284 and 1401 A.D. and 1216 and 1383 A.D., respectively. Near the truncation of terrace Qt4 by the HFT, a sample of detrital charcoal (LRT-01, **Figure 4**) is collected below the active soil from a pit excavated on the Qt4 surface (**Figures 4, 5**). The pit exposed sub-rounded, well-sorted fluvial gravels (Unit 1) overlain by fine-grained overbank deposits (Unit 2) consisting of a fining upward sequence of sand to silty clay deposits with interbedded coarse sand lenses (**Figure 5**). A silty sand layer containing abundant pottery shards and disseminated charcoal fragments (Unit 3) caps the entire exposure. A distinct burnt layer marks the base of Unit 3. The charcoal fragment we dated (LRT-01) was collected from Unit 2 at ~1.9 m depth below the present day surface. The age of the sample is 1035 – 1207 A.D. (LRT-01, Table 1). The observation places a maximum age of about ~ 900 years on the Qt4 surface.

The Qt4 terrace sits 20 m – 32 m above active stream grade while the modern Qt5 surface that is not cut by the HFT sits 15 m above active stream grade. The 15 m of incision is historical and probably induced by gravel mining in the upstream reaches of the Ghaggar River, subsequent to the last surface rupture event along the HFT. Near the HFT, the bedrock incision of Qt4 and Qt5 terrace surfaces are 20 and 8 m, respectively, above current stream grade. If we assume the difference between the two, 12 meters, is the result of uplift due to multiple earthquakes between 1035 and 1207 A.D. (maximum age of the Qt4 surface; sample LRT-01), we arrive at an estimate of the uplift rate along the fault of 10.7 ± 0.8 mm/yr.

We excavated a ~40 m long and 4-5 m deep trench (**Figure 6**) across the fault where it cuts the Lower River Terrace Surface (Qt4) near the city of Chandigarh (**location of trench on Figures 3, 4**). The trench was located inside the Government College campus in Panchkula, where the fault strikes northwest and is expressed by a ~1.8 m high scarp (**Figure 4**). The northeastern end of the trench exposes four units in the hanging wall. The oldest and lowest (Unit 1) is a layer of sub-rounded, well-sorted, clast supported cobble gravel of fluvial origin. Unit 2 is well-sorted matrix supported fluvial cobble gravels. Unit 3 is sub-rounded, well-sorted pebble-cobble gravels of fluvial origin. The uppermost and youngest sediments on the hanging wall (Unit 4) consist of a thick mantle of extensively bioturbated silty sand overbank deposits. At the crest of the topographic scarp, the flat lying hanging wall units bend abruptly downward and dip 12° to the southwest. The bend marks the crest of the surface scarp and is associated with two normal faults (F2 and F2') which form a graben and presumably accommodate bending associated with folding of the hanging wall. In between faults F2 and F2' and southwestward the hanging wall units dip to form a

ramp that parallels the surface expression of the scarp. The southwestern limit of the hanging wall units is marked by a basal thrust fault (F1). The thrust has transported the hanging wall Units 1-3 and 4' onto the footwall Unit 4. The faulted footwall Unit 4 is also observed on the hanging wall. Alternating thin beds of pebbles and fine- to medium-grained sand comprise a cut and fill fluvial channel that caps both the foot and hanging wall units (Unit 5). Unit 4' is interpreted to be the basal remnant of Unit 4 on the footwall or possibly an older cut and fill deposit analogous to Unit 5. Pebble-cobble gravel oriented randomly in a massive silty sand matrix (Unit 6) probably represents scarp-derived colluvium. The uppermost and youngest sediments consist of alternating thin beds of fine- to medium-grained silty sand of overbank flood deposits (Unit 7).

Radiometrically determined AMS ages of detrital charcoal place limits on the time of displacement registered across the thrust fault F1. Unit 4 is cut by the fault F1. The ages of four detrital charcoal samples collected from Unit 4 range in age from 762 B.C. - 1628 A.D. (PAN-05, PAN-08, PAN-23, and PAN-28; **Table 1 & Figure 6**). Sample PAN-08 is interpreted to be reworked detrital charcoal on the basis of its older age as compared with sample PAN-05 from the same stratigraphic level. Samples PAN-23 and PAN-26 collected near the top of Unit 4 are younger in age, 1299 – 1413 A.D. and 1404 – 1628 A.D. The stratigraphic inversion of the two dates indicates the samples are reworked detrital charcoal. The correlation of Unit 4 across the fault is supported by similarities in radiocarbon ages taken from samples in the footwall (PAN-05, PAN-23, and PAN-26 in **Figure 6**) and hanging wall (LRT-01 in **Figure 4 & 5** & natural exposure samples GAG-03 and GAG-05 in **Figure 4**) portions of the unit. That is to say, the ages of PAN-23 and PAN-26 are similar

to those found for the Qt4 terrace surface that is cut by the HFT. Taking the youngest age of reworked detrital charcoal as a maximum limiting age of Unit 4, the most recent slip on F1 is interpreted to have occurred after 1404–1628 A.D. Units 5 and 6 post-date the displacement on F1. The ages of four samples (PAN-01, PAN-02, PAN-03, and PAN-27) collected from the basal portion of colluvial Unit 6 range in age from 683 to 1950 A.D. The range of ages obtained for Unit 6 overlap with the ages of PAN-23 and PAN-26 in underlying Unit 4. The samples in Unit 6 may be reworked from older hanging wall deposits. For these reasons, it is difficult to place a firm upper bound for displacement on F1. Toward that end, we draw upon a separate observation that Pinjore Garden, located about 10 km to the northeast of the fault, has not incurred any damage from earthquakes since it was built during the 17th century A.D. (http://www.haryana-online.com/pinjore_gardens.htm) (**Figure 3**). Based on this observation and coupled with the radiocarbon dates of faulted and unfaulted deposits observed in trench exposure, we suggest that displacement on F1 must be result of an event that occurred post 1404–1628 A.D. (PAN-01; **Table 1 & Figure 6**) but before the Pinjore Garden was built during the 17th century A.D.

A minimum of 2.3 m of slip is recorded in the trench exposure by the thrusting of Units 1, 2, 3, and 4' over Unit 4 (**Figure 6**). More slip is required to explain the dip panel and apparent vertical separation across the fault. For example, vertical separation across fault F1 between the surface at the time of the most recent event, represented by the faulted Unit 4, and the present-day hanging wall surface, also Unit 4, is 4.4 m (**Figure 6**). If we assume that 29° dip on the fault F1 continues to depth, then 9.1 m of dip slip is required to produce 4.4 m of observed vertical separation. We think the scarp is due to a single

displacement, but the possibility exists that Unit 4' is a cut and fill deposit analogous to Unit 5 allows the possibility that it represents an earlier event and the vertical separation is the sum of two events. If we assume vertical uplift during last event was 4.4 m, then dividing the vertical separation of 4.4 m across the scarp by the minimum vertical uplift rate of $> 10.7 + 0.8$ mm/yr determined from the Qt4 terrace yields $\leq 441 \pm 15$ years to accumulate sufficient slip to produce similar size displacements. If the scarp was result of two earthquakes then the estimated time to accumulate slip to produce similar size displacements would be smaller.

KALA AMB (SITE 2)

Kala Amb is located ~40 km to the southeast of Chandigarh and between the longitude $77^{\circ} 10'$ and $77^{\circ} 14'$ E (**SITE 2 in Figures 2, 7**). The trace of the HFT takes a sharp right step near the town of Kala Amb (**Figure 7**). The step in the fault trace is a tear fault expressed by a clear scarp in alluvium that truncates and uplifts terraces along the Markanda River (Kumar et al., 2001; **Figure 7**). In contrast, scarps in Quaternary alluvium are not distinct along the main trace of the HFT near Kala Amb. Displacement on the underlying HFT to the south has produced an asymmetric south-verging anticline within the Siwalik Group in the hanging wall (**Figure 7**). Near Kala Amb, Siwalik beds on the backlimb of the anticline show northerly dips ranging between 20° and 40° . Dip directions reverse and are as steep as 60° to the south on the forelimb of the anticline (Srivastava et al., 1981).

The Markanda River terraces are the result of multiple earthquake displacements, and provided Kumar et al. (2001), the basis to establish a minimum bound on the uplift rate due to slip on the HFT of 4.8 ± 0.9 mm/yr based on a radiocarbon age of 4896 ± 68 cal. years B.P. for the terrace surface (**Figure 8**). The uplift rate equates to fault slip and crustal shortening rates of $9.6 \frac{+7.0}{-3.5}$ mm/yr and $8.4 \frac{+7.3}{-3.6}$ mm/yr, respectively assuming that the HFT dips at $30^\circ \pm 10^\circ$ (Kumar et al., 2001).

Kumar et al. (2001) report evidence from a trench exposure of two and possibly three surface rupture earthquakes that have resulted in cumulative coseismic slip of 8.6 meters on the tear fault during the last 600 years. The two most recent earthquakes occurred subsequent to 1294 A.D. and 1423 A.D., respectively, and possibly another rupture at about 260 A.D. Minimum displacements during the post-1294 A.D and post-1423 A.D. events were on the order of 5.3-5.4 m and 2.4-4.0 m, respectively, and a possibly larger displacement interpreted for the 260 A.D. event (Kumar et al., 2001). The slip occurred on fault strands dipping 9° to 12° and is insufficient to account for the vertical separation (~ 7.2 m) across the fault. Hence, near-surface folding of surficial layers accommodated much of the permanent strain at the ground surface.

RAMPUR GANDA (SITE 3)

The Rampur Ganda study area is located approximately 20 km east of **Site 2** (Kala Amb), and is labeled **Site 3** in **Figures 2, 7**. Here the trace of the HFT is discontinuously expressed as fault scarps in Quaternary alluvium. We placed a ~ 58 m long trench across a remnant east-west trending ~ 13 m high scarp near the outlet of the Somb River near the

small village of Rampur Ganda (**Figure 7**). A log of the eastern trench wall is shown in **Figure 9**. The northernmost hanging wall portion of the trench is composed of two distinctive units. The oldest and lowest (Unit 1) is a highly sheared and faulted package of middle Siwaliks sandstone and mudstone. The shear fabric on the Siwaliks increases in intensity toward the south and appears to be the result of repeated tectonic activity. Unit 2a is a well- to sub-rounded, poorly-sorted fluvial sand, cobble and boulder gravel that caps Unit 1 along an erosional unconformity. The uppermost and youngest sediment on the hanging wall (Unit 2b) is clayey silt to medium sand overbank deposits that shows a weak to moderate soil horizonation. The unit is about ~2 m thick to the north and tapers out to only centimeters in thickness near the inflection of the topographic scarp, after which it disappears entirely due to erosion of the scarp. The flat lying units of the hanging wall bend gradually downward to a maximum dip amount of 16° to the south. The bend marks the inflection of the surface scarp and is associated with tensional cracks (F4 and F4'), which form a graben and presumably accommodate a portion of the bending (**Figure 9**). The dipping hanging wall units form a ramp that parallels the surface expression of the scarp. A basal thrust fault (F1) marks the southern limit of the hanging wall. The fault strand F1 has transported the hanging wall units (Unit 1, 2a, and 2b) over footwall unit 2b'. The lowermost of the footwall units exposed in the trench (Unit 2b') consists of dark gray, organic rich clayey silt to medium sand. The Unit 2b' is faulted and contains abundant charcoal and pottery shards, and capped by a weak and buried soil horizon. The unit is interpreted to be the ground surface at the time of the fault displacement on F3. An unfaulted package of medium to coarse sand with occasional pebbles caps both the foot and hanging wall units (Unit 3). The Unit 3 is distinguished by thinly (0.5-2 mm) laminated,

discontinuous (30-40 cm) sand beds, mostly planar but with occasional fine laminations, which we interpret to be aeolian accumulation or reworking of moderate to coarse sand at the base of the fault scarp. The uppermost and youngest sediments (Unit 3') consist of fine to medium clayey package with occasional pebble-cobble gravels oriented randomly and is interpreted as scarp-derived colluvium.

Fault strand F2 cuts to within a meter from the surface and disrupts the sediments of Unit 2b but not the capping Unit 3 and 3' (**Figure 9**). Fault strand F3 exhibits minor displacement (0.5 m) and cuts Units 1-2a, and transfers slip to and merges with the main strand F1. Fault strand F1 warps and truncates the hanging wall units but not the capping units 3 and 3'. Displacement of ~5.1 m along the fault strand F1 resulted in warping and sliding of the hanging wall at very low angle and shearing and ploughing of Unit 2 and soil horizon (Unit 2b'). Shearing and ploughing of sediments was accompanied by brittle displacement along fault strand F1 that transported hanging wall units (Unit 1, 2a and 2b) over the sheared and bulldozed sediments now preserved immediately beneath the snout of the upward termination of fault strand F1. Displacement on F1 was followed by aeolian deposition of Unit 3 against the fault scarp and emplacement of the scarp-derived colluvium of Unit 3'.

Radiometric ages determined for detrital charcoal place limits on the timing of displacement registered across the thrust fault strands F1-F3. The detrital charcoal sample AB-07 recovered from youngest faulted soil horizon (Unit 2b') limits the most recent fault displacement to after 1222-1380 A.D. (**Table 1 & Figure 9**). Sample AB-08 collected from the oldest unfaulted Unit 3 limits the most recent earthquake to before 1319-1442 A.D.

When taken together, radiocarbon dates and fault relations suggest that the fault traces F1, F2, and F3 occurred in one earthquake during the past ~700 years, between 1222 and 1442 A.D. A detrital charcoal sample (AB-18, **Table 1**) recovered ~1 m below surface of Unit 2b near the northern end of the trench in the hanging wall provides a radiometric age of 439–641 A.D. We interpret the upper contact of Unit 2b on the hanging wall and Unit 2b' on the footwall to have been the ground surface prior to faulting. The disparity in the ages of radiocarbon samples obtained from Unit 2b' (sample AB-07) and Unit 2b (sample AB-18) reflects that AB-07 is taken from a paleosol that caps Unit 2b whereas AB-18 is taken from within Unit 2b. The portion of Unit 2b that now sits above Unit 2b' on the footwall was emplaced tectonically by plowing and displacement at the tip of the fault F1.

Total displacement recorded during the earthquake is ~6.8 m, with 5.1 m, 1.2 m and 0.5 m on strands F1, F2, and F3, respectively (**Figure 9**). The surface at the time of the earthquake represented by faulted Unit 2b' and the uplifted terrace surface of the hanging wall are interpreted to have been continuous prior to faulting and now exhibit a vertical separation of 7.5 m (**Figure 9**). Fault strands F1, F2, and F3 show a steep dip ranging between 30° and 33° near the base of the trench but tend to flatten to roughly horizontal near their tips. Assuming a dip of 30° continues at depth and all the deformation observed in F1, F2, and F3 strands is attributed to a single event, a displacement of 15 m along the fault is required to explain the 7.5 m of vertical separation between Units 2b on the hanging wall and 2b' on the footwall. Restoration of brittle displacement recorded on fault strands F1, F2, and F3 only explains for 1.5 m of the total 7.5 m vertical separation. The discrepancy in the measurement indicates that much of the displacement is accommodated in folding and tilting

of the hanging wall with a small portion taken up by formation of extensional crack in the hanging wall, in addition to fault displacement along F1. Thus the total fault displacement of 6.8 ± 0.1 m recorded by F1, F2, and F3 strands provide a minimum measure of fault slip for the earthquake. Vertical separation of 7.5 m divided by the long-term vertical uplift rate of $\geq 4.8 + 0.9$ mm/yr obtained for nearby uplifted Markanda river terraces in Kala Amb (Kumar et al., 2001) yields an estimate of $\leq 1619 \pm 304$ years to accumulate the slip released during the last surface rupture at Rampur Ganda.

DEHRADUN (SITE 4)

Displacement along the southernmost north dipping HFT, near Dehradun, locally referred to as the Mohand Thrust, has produced a broad south-verging anticline within the Siwalik Group in the hanging wall (Rao et al., 1974; Raiverman et al., 1993; Thakur, 1995; Wesnousky et al., 1999) (**Figures 2, 10**). Siwalik beds on the back limb of the anticline show northerly dips ranging between 20° and 30° . Dip directions reverse and are as steep as 45° to 70° to the south on the forelimb of anticline (Thakur and Kumar, 1995). Continuous fault scarps in Quaternary alluvium are not evident along the main trace of the HFT between the town of Mohand and the Yamuna River (Nakata, 1972; Nakata, 1989) (**Figure 10**). However, prior drill hole data, seismic reflection profiles (Rao et al., 1974; Raiverman et al., 1993), and short discontinuous fault scarps near the Chapri Rao and the Tybryon village (Wesnousky et al., 1999) suggest that the fault is emergent near the study area (**Figure 11**).

The distribution of fluvial terrace deposits has previously been mapped by Wesnousky et al., (1999) and shown in **Figure 11**. Two levels of uplifted and truncated fluvial terrace deposits are recognized along the ephemeral streams issuing from the sub-Himalayas between the Khajnawara and Yamuna River (Wesnousky et al., 1999). Surveys of the Khajnawara and Shajahanpur terraces show they are not measurably warped or folded where exposed within the ~2 km of the rangefront. The lack of warping is consistent with the interpretation that the hanging wall undergoes a rigid translation along the underlying HFT. The highest terraces at Khajnawara and Shajahanpur Raos are 20 to 30 meters above current stream grade. A radiometric age limits the age of the higher terrace to $\leq 3663 + 215$ radiocarbon years before present, yielding a vertical uplift rate of $\geq 6.9 + 1.8$ mm/yr (Wesnousky et al., 1999). A shortening rate of $\geq 11.9 \pm 3.1$ mm/yr across HFT and the slip rate of $\geq 13.8 \pm 3.6$ mm/year for the HFT is estimated based on the geometrical constraint that the HFT dips northerly at about 30° near Mohand (Rao et al., 1974; Raiverman et al., 1993).

We placed a series of trenches within the streambed of Khajnawara Rao and Shajahanpur Rao (**Figure 12**). The trenches show that the HFT reaches to the surface, covered by only a thin strath deposit in the active streambeds. A representative example of the series of trenches is shown in **Figure 12 (Trench ZT -02)**. The trench is located near the mouth of Khajnawara Rao along the projection of adjacent truncated higher terraces south of the Siwalik range front (**Figure 12**). The oldest unit exposed is highly sheared Siwalik bedrock (Unit 1). The Siwalik bedrock (Unit 1) is thrust over alluvial pebble-cobble gravels in a clayey silt to sandy matrix (Unit 2) along a well-defined low angle thrust fault strand (**Figure 12**). The faulted Units 1 and 2 are capped along an erosional unconformity

by unfaulted alluvial gravels consisting of poorly sorted small pebble to small cobble gravels in medium to coarse sand matrix (Unit 3a). The gravels of Unit 3a are modern deposits currently being transported down the Khajnawar Rao during monsoons. A wedge shaped talus deposit (Unit 3b) from the adjacent hillside is observed near the northern end of the trench, and a very thin mantle of modern overbank deposits (Unit 3c), caps Units 3a and 3b (**Figure 12**).

Scars in young alluvium are not present at the surface along the projection of the fault, and stratigraphic relations in the trench show complete removal of the fault scarps by fluvial processes within the streambeds. The boundary between Siwalik bedrock and alluvial deposits of the floodplain is abrupt and steep. Based on the occurrence of Siwalik bedrock overriding young alluvial deposits along a low-angle thrust fault in trench ZT-02, we conclude that repeated earthquakes on an emergent fault have formed the adjacent abrupt and steep escarpments that are characteristics of this section of the rangefront.

LAL DHANG (SITE 5)

Lal Dhang is located ~50 km east of Dehradun (**Site 5 in Figure 2**). The trace of the HFT is expressed as fault scarps in Quaternary alluvium near the village of Lal Dhang (**Figure 13**). The Siwalik Hills on the southeastern portion of the map show northeasterly dips generally ranging between 25° and 60° (Rupke, 1974). A trench excavated perpendicular to a northwest trending scarp near the village of Lal Dhang exposed the HFT (**Figure 13**). The oldest unit exposed by the ~25 m long and 4 to 6 m deep trench is an alluvial fan gravel sequence (Unit 1), composed mainly of sub-rounded to rounded cobble to

boulder gravel with interbedded lenses of sand (**Figure 14**). Units 2 - 5 lie conformably on the fan gravels of Unit 1 and extend sub-horizontally across the entire base of the trench exposure. Unit 2 is a well-sorted, strongly stratified, and poorly compacted pebble-cobble gravel deposit. Unit 3 consists of alternating layers of poorly compacted sand and silty sand deposit of fluvial origin. Unit 4 is hard, massive silty clay and Unit 5 is a thin but distinctive sandy silt deposit characterized by rich organic matter and pottery shards. Units 1 - 5 are repeated higher in the trench wall, where they are deformed by folding and shearing, and are warped along fault strand F1 (**Figure 14**). Unit 6 is the basal horizon of unfaulted colluvium that consists of poorly laminated massive silty clay, which we interpret to be reworked hanging wall deposits accumulated at the base of the fault scarp. Scarp-derived colluvium (Unit 7) is composed of randomly oriented and poorly sorted pebble-cobble gravel in a silty sand matrix and runs nearly the entire length of the trench exposure. A very thin channel is emplaced within the colluvial layer (Unit 7a) near the southwestern end of the trench.

Fault strand F1 warps and drags units 1 through 5 on the hanging wall. Unit 6 is not faulted or warped. Thus, the top of Unit 5 is interpreted to have been the ground surface at the time of displacement along fault strand F1. The hanging wall has slipped at very low angle onto the former ground surface (Unit 5) and bulldozed sediments and soil in front of the lip of the overthrust block. The deformation has resulted in duplication of Units 2, 3, and 4 along the front of the thrust. Three detrital charcoal samples were collected and dated from the faulted Units 3 and 4. Detrital charcoal samples LDT-02 and LDT-15 obtained from Unit 3 predate the fault displacement and yield dates between 1069 and 1261 A.D. (**Table 1 and Figure 14**). Sample LDT-11, obtained from the faulted Unit 4, provides a

maximum date of 1282 to 1395 A.D. for the fault displacement. Two radiometric ages of detrital charcoal samples obtained from the unfaulted Unit 6 (LDT-43 and LDT-31) range in age between 1306 and 1632 A.D. and postdate the fault displacement. Detrital charcoal sample, (LDT-32), obtained from the colluvial wedge (Unit 7) yields an age 1436 to 1614 A.D. and is in similar age range for the samples obtained from Unit 6 (**LDT-43 and LDT-31, Table 1 and Figure 14**). Taken together, radiometric ages of detrital charcoal obtained from faulted and unfaulted deposits exposed in the Lal Dhang trench show that displacement observed along fault trace F1 is the result of a single surface rupture that occurred after 1282 and before 1632 A.D.

The near horizontal orientation of fault strand F1 and the bulldozing and deformation of sediments indicates proximity to the tip of a thrust. The thrust must steepen at depth to have cut and transported Units 1-5. The tilting of Unit 1 to produce a dip panel parallel to the scarp slope and the presence of a single colluvial wedge indicates the fault scarp is due to a single event. Vertical separation between top of the surveyed hanging wall surface and the surface at the time of faulting (Unit 5) in the footwall is 9.0 m (**Figure 14**). Assuming that the fault steepens at depth to dip 30° as observed in Chandigarh, Kala Amb, and Rampur Ganda, 18 meters of displacement is required to explain the observed 9.0 m of vertical separation. Since the fault is sub-horizontal, restoration of ~7 m brittle displacement recorded in the trench on fault strand F1 will yield an insignificant value to explain the vertical separation. The discrepancy in the measurement indicates most displacement is accommodated in near-surface folding and tilting and production of the dip-panel that forms the scarp. If we assume a rate of long-term uplift similar to that observed at Shahajanpur,

Dehra Dun ($\geq 6.9 \pm 1.8$ mm/yr) it would on average take $\leq 1417 \pm 383$ years to accumulate slip to produce the 9 m of vertical separation we observe at Lal Dhang.

RAMNAGAR (SITE 6)

Near Ramnagar (**Site 6 in Figure 2**), displacement along the southernmost north dipping HFT has produced a broad south-verging anticline within the Siwalik Group (Rao et al., 1973) (**Figure 15**). The Siwalik Hills on the western portion of the mapped area (**Fig 15**) comprise mainly homoclinal strata with dips on the northern flank generally ranging between 15° and 30° . Dip directions reverse and are as steep as 70° to the south on the forelimb of the anticline. To the east of the Kosi River, Siwalik beds take a sharp right step to the south of Dabka River. To the southeast of Dabka River, dip directions on the backlimb of the Siwaliks show northerly dip ranging from 10° to 20° , whereas the south-side of the forelimb of the anticline show dips ranging from 30° to 60° (Rao et al., 1973). Fault scarps in Quaternary alluvium are present along the main trace of the HFT within the mapped area (Nakata, 1972) (**Figures 15, 16**). The HFT is expressed as relatively continuous fault scarp in alluvium between the Swaldeh River and Kosi River. East of the Kosi River, the HFT is discontinuously expressed and takes a right step toward the south along the Siwaliks.

Terraces offset by the HFT along the Kosi River occur on both the banks of the Kosi River (Nakata, 1972; **Figures 15, 16**). All the terrace surfaces are truncated by the ESE trending HFT. The oldest surface, Qt₁, sits about 65-90 m above the present riverbed

(Figure 16). The intermediate aged strath terrace deposits (Qt2) are about 15 m thick, with terrace surfaces and bedrock-alluvium strath contacts at about 50 and 35 m above the present riverbed, respectively (**Figure 16**). The Lower River terraces (Qt3) are about 14 m above present river grade and are generally capped by a thin strath of fluvial gravels and overbank deposit on the gently dipping Siwalik bedrock strath (**Figure 15**). Terrace surface, Qt3, occurs along the smaller ephemeral streams that issue from the Siwalik Hills, and a broad remnant of the surface is locally preserved along the Swaldeh, Chor Pani, and Karkat River.

We excavated a 2 m deep pit on the Middle River Terrace (Qt2) a few kilometers north of Ramnagar near the village of Ringora (**Figure 16**). The oldest deposits exposed in the pit (**Figure 16**) are sub-rounded, well-sorted fluvial gravels (Unit 1). The gravels of Unit 1 are capped by bioturbated fine-grained overbank deposits of clay to silty sand (Unit 2). Radiometric dates of two detrital charcoal fragments (KMRT-03 and KMRT-07; **Table 1 and Figure 16**) collected from Unit 2 about 1.6 m below the present-day surface limit the age of the terrace surface to 3906-3701 B.C. and 5620-5485 B.C., respectively. Detrital charcoal samples were purposely recovered from near the contact of the fluvial gravel and overlying cap of overbank deposits to avoid sampling of reworked charcoal. Although the location of samples suggests original deposition, the presence of termite mounds and lack of primary sedimentary structures raise concern that the detrital charcoal may have been emplaced subsequent to terrace formation. Assuming the samples KMRT-03 (3906-3701 B.C.) and KMRT-07 (5620-5485 B.C.) ages are close in time to the formation of the Qt2

surface, a range of uplift rates of 6.6 to 8.8 mm/yr is obtained by dividing the sample age values in to the 50 m uplift of Qt2 surface above the present stream bed.

We opened a ~32 m long trench perpendicular to the fault where it cuts the Lower River Terrace (Qt3) near the village of Belparao (**Figure 16**). At this location, the fault strikes east-west and is expressed by a ~13.0 m scarp. A detailed log of the western trench wall is provided in **Figure 17**. Five distinct units exposed (Unit 1 through 5) from base to top span the entire length of the trench. The oldest exposed unit at the base of the trench is rounded- to well-rounded, poorly stratified sand and medium boulder gravels (Unit 1). Unit 2 is a distinctive, mottled light tan to yellow sandy clay layer. Unit 2 shows a facies change towards the northern end of the trench, where medium to coarse-grained sand to pebble gravel channels can be correlated on opposite walls of the trench and indicate scarp parallel paleo-flow direction. Overlying Unit 2 is clayey medium- to coarse-grained sand (Unit 3). Occasional discontinuous gravel stringers and increasing clay content towards the top of the unit distinguishes Unit 3 from Unit 2. Unit 4 is clayey silt to coarse sand distinguished by well-defined thin channels. The top of the unit is oxidized and shows red coloration. The youngest and uppermost unit is a dark clayey sand package (Unit 5). The unit shows weak soil structure and few randomly oriented pebbles and cobbles and interpreted as scarp-derived colluvium (Unit 5). All of the exposed units, with the exception of Unit 5, are cut and deformed by thrust fault strands, F1, F2, and F3 (**Figure 17**). The exposed sediments dip 16° to the south and parallel the surface expression of the fault scarp.

The northernmost of the fault strands, F3 strand, splays into three slivers that displace and deform Units 1-4 (**Figure 17**). Fault strand F2 displaces and folds all units except Unit 5. The southernmost fault strand, F1, also displaces and folds all units but Unit 5. Fault strands F1, F2, and F3 record displacements of 1m, 1.4m, and 1.4m, respectively (**Figure 17**).

Detrital charcoal sample BR-09 obtained from faulted Unit 2 and predates the fault displacement and is dated at 984 - 1158 A.D. (**Figure 17; Table 1**). Sample BR-15 collected from the overlying faulted Unit 3 provides a radiometric age of 1259-1390 A.D., and sample BR-18 recovered from the youngest faulted package (Unit 4) yields an age of 1278-1390 A.D. (**Figure 17; Table1**). Thus the detrital charcoal sample BR-06 collected from the youngest faulted Unit 4 provide radiometric age that limit faulting at after 1278-1390 A.D. Detrital charcoal (sample BR-07; **Table 1**) collected from the unfaulted colluvial package (Unit 5) limits the most recent earthquake to before 1301-1433 A.D. In sum, a total brittle displacement of 3.8 m recorded along fault traces F1, F2, and F3 is interpreted to be the result of one earthquake that occurred ~700 years ago, between 1278 and 1433 A.D.

The surface at the time of the most recent earthquake, represented by faulted Unit 4 in the footwall, and the surface of the present-day terrace on the hanging wall are separated at least by 13.0 m (**Figure 17**). The fault strands F1, F2, and F3 show dip amounts ranging between 16° and 33°. Assuming a dip of 30° continues at depth, dip slip of ~ 25 m along the fault is required to explain the 13.0 m of vertical separation. Restoration of brittle displacement recorded on fault strands F1, F2, and F3 only explains a small portion of the total 13.0 m vertical separation. The disagreement between the amount of offset observed

along visible fault traces and the displacement required to produce 13.0 m of vertical separation indicates that most of the strain is accommodated by tilting and folding of the hanging wall, in addition to fault displacement along F1. If the vertical separation of 13.0 m across the scarp is divided by a range of long-term uplift rate of 6.6 to 8.8 mm/yr obtained for the uplifted Qt2 Kosi river terraces (**Figure 16**), then it yields an estimate of 1477 to 1969 years (1723 ± 246 years) to accumulate sufficient slip to produce similar sized displacements at Ramnagar.

CHOR GHALIA (SITE 7)

Chor Ghalia is located approximately 65 km east of Ramnagar (**Site 7, Figure 2**). Near the village of Chor Ghalia, fault scarps in Quaternary alluvium are evident along the main trace of the HFT, while, directly east of Chor Ghalia the scarps are discontinuous and eroded by the Nandaur River (**Figure 18**). Two prominent fluvial terrace deposits and a modern alluvial fan surface are preserved along the Nandaur River: the Higher River Terrace (Qt1), the Lower River Terrace (Qt2), and the Modern fan Surface (Qt3) (**Figure 18**). The NW–SE striking HFT truncates Higher River (Qt1) and Lower River (Qt2) terrace surfaces but not the Modern fan surface (Qt3). The oldest surface, Qt₁, sits about 50 m above the present riverbed and is capped by a ~20 m fluvial boulder gravel strath deposit. The Lower River Terrace surface (Qt2) sits approximately 20 m above the present riverbed and is characterized by a thin veneer of fluvial boulder gravel. The Modern River Terrace (Qt3) surface also forms an alluvial fan outboard of the rangefront to south of the HFT and sits about 7 m above the present Nandaur River grade. We excavated a 6 m deep pit on the

Higher River Terrace (Qt1) approximately two hundred meters northwest of the village of Chor Ghala (**Figure 18**). The oldest deposits exposed in the pit (**Figure 18**) are silty sands with abundant pottery shards (Unit 1). A thick clast supported cobble-boulder gravel layer (Unit 2) overlies Unit 1. The unit is distinguished by occasional large pieces of pottery fragments disseminated within cobble-boulder clasts. Presence of pottery fragments disseminated within the stratigraphic Units 1 and 2 suggests original deposition while the surface was still an active floodplain.

A radiometric date obtained from a detrital charcoal fragment (**NHRT-03 Table 1 and Figure 18**) located 5 m below the terrace surface within Unit 1 provide a maximum age of the terrace surface of 476-262 B.C. A reliable estimate of uplift rate from the elevation of the Qt1 terrace above stream grade is hampered by significant amount of Qt3 terrace incision outboard the range front during modern time and subsequent to the last surface rupture along the HFT. Near the HFT, the Qt1 and Qt3 terrace surfaces are 30 m and 7 m above current stream grade. If we assume the difference between the two, 23 m, is the result of uplift due to multiple earthquakes between 476 and 262 B.C. (maximum age of the Qt1 surface), we arrive at a vertical uplift rate of 9.8 ± 0.4 mm/yr. along this stretch of the HFT.

DISCUSSION & CONCLUSIONS

Is the HFT blind?

Displacement along the underlying north dipping HFT has produced an asymmetric south-verging anticline within the Siwalik Group in the hanging wall. This structure has been attributed to fault-bend or fault propagation folding (Raiverman et al., 1993; Thakur, 1995; Powers et al., 1998). The folding of Siwalik bedrock north of the HFT, and the occurrence of large historic earthquakes that apparently have not broken the surface, has been the basis to suggest that the HFT is a blind thrust (Stein and Yeats, 1989; Yeats et al., 1992; Yeats and Thakur, 1998). Lack of apparent surface expression of the HFT has also led some workers to believe that the HFT is “concealed” by Quaternary deposits or eroded (Raiverman et al., 1993; Valdiya 2003). Our observations gained from shallow trenches excavated at 6 sites along a ~400 km section of the Indian Himalaya show that the HFT is emergent and that ruptures commonly break young surficial deposits. Although the anticlinal form of the Siwaliks appears to be the result of a fault-bend or fault propagation folding during the earlier stages of development of the Indian HFT, we suggest that today the system has matured and displacement of the Indian Siwaliks is largely approximated as a rigid block displacement on the HFT that reaches the surface. Additionally, the surface faulting at six shallow trenches along the Indian HFT is on strike with the abrupt and steep contact between the Siwalik rangefront and alluvial sediments of the Indo-gangetic plain. In

that regard, the abrupt front of the Siwaliks appears to closely mark an emergent fault contact along the entire Indian Himalaya.

Uplift, fault slip and shortening rates

The long-term geologic expression due to the rigid block displacement on the HFT has resulted in the occurrence of uplifted and truncated fluvial strath terraces of varying height and age near the mouths of the Ghaggar, Markanda, Shajahanpur, Kosi, and Nandaur rivers (**Figures 4, 7, 11, 16, and 18**). Minimum long-term vertical uplift rates obtained by dividing the elevation of the fluvial strath terraces by the radiometric age obtained for the terrace deposits at the respective sites yield rates that range from about 5 to 11 mm/yr (**Figures 4, 7, 11, 16, and 18**). The rates are expressed as minimum because the radiocarbon ages are maximums for the uplifted surfaces. If an average 30° dip for the HFT is assumed, the long-term vertical uplift rates correspond to a minimum fault slip rates of 10 to 22 mm/yr and shortening rate of about 9.0 to 19.0 mm/yr at the respective study sites. The rate of shortening is similar to rates reported elsewhere along the HFT based on the offset of late Pleistocene and Holocene sediments (**Table 2**; Wesnousky et al., 1999; Lave and Avouac, 2000; Kumar et al., 2001). The shortening rate we estimate is also in general agreement with shortening rates based on retro-deformation of Mio-Pliocene rocks (**Table 2**; Lyon-Caen and Molnar, 1985; Leathers, 1987; Baker, 1988; Pennock et al., 1988; Schelling and Arita, 1991; Schelling, 1992; Avouac and Tapponnier, 1993; Jaswal et al., 1997; Powers et al., 1998); shortening rates estimated from analysis of historical earthquakes (**Table 2**; Molnar and Deng, 1984; Molnar, 1990); and rates of shortening based

on yet shorter records of GPS measurements (**Table 2**; Jackson & Bilham, 1994; Freymueller et al., 1996; Bilham et al., 1998; Paul et al., 2001; Banerjee and Burgmann, 2002). The similarity in shortening rates calculated over a broad range of time scales suggests that convergence across the Himalayan front has occurred at a relatively steady rate through time.

Timing and extent of paleoearthquakes

We present in **Figure 19** a space-time diagram showing the trench sites located between Chandigarh in the west to Ramnagar in the east along a ~400 km stretch of the Indian HFT. The horizontal axis is distance and the scale is same as in overlying map. The vertical axis is time in years A.D. The vertical bars with bounding dashes represent the range of limiting ages of past surface ruptures at the respective study sites. The sites fall within the central seismic gap (>800 km) defined by Khattri (1987) and bounded by the rupture zones of the 1905 Kangra ($M_s \sim 7.8$) and the 1934 Bihar-Nepal earthquake ($M_w = 7.7 \pm 0.2$) (**Figure 1**). No large historical earthquakes are reported within the central seismic gap (**Figures 1, 19**) for at least 200 years and perhaps for as long as ~700 years (Bilham et al., 1995).

The plot show ages of the most recent events recorded at all of the sites to overlap within the uncertainties of the radiometric age. This when combined with the large coseismic offsets observed in the trenches, the incompleteness of historical records (Bilham et al., 1995), and the apparent youthfulness of the scarp and associated fractures allow possibility that the younger slip event recorded in all sites is due to a through-going rupture

that broke at least \sim 400 km of the Indian HFT. If the most recent event preserved in our trenches is due to a through-going earthquake and if the age of that event is accurately constrained by our radiometric dates, then the event can be interpreted as having occurred where the dates overlap, or between 1404-1422 A.D (**Figure 19**).

The northwesternmost Chandigarh (SITE 2) and Kala Amb (SITE 3) show evidence for multiple earthquakes and perhaps are sites of overlapping ruptures (**Figure 19**). Observations from a trench exposure on a tear fault near Kala Amb (SITE 2) show evidence for two and possibly three earthquakes with the two most recent earthquakes occurred during the last \sim 650 years. (Kumar et al., 2001) (**Figure 19**). The most recent event dated between 1424 and 1950 A.D. overlaps with the 1404 – 1422 A.D. event recorded in the Chandigarh, Rampur Ganda, Lal Dhang, and Ramnagar trenches. Kumar et al (2001) speculated the most recent event recorded in the Kala Amb as the 1905 Kangra earthquake based on incompleteness of historical reports and observed youthfulness of the scarp and associated fractures.

Evaluation of earthquake size, rupture length and repeat time

Assuming a fault dip of 30° for the HFT at depth and using vertical separation values of 7.5 m, 9.0 m, and 13.0 m obtained from scarp profiles of Rampur Ganda, Lal Dhang and Ramnagar (**Figures 10, 14, 17**), we interpreted single-event slips of 15 m, 18 m, and 25 m, respectively. The dip-slip displacement of 15 to 25 m is comparable to the average dip-slip displacement of \sim 12 m and \sim 19 m calculated for the large plate boundary events such as the

1964 Southern Alaska earthquake (M_w 9.2) and the 1960 Southern Chile earthquake (M_w 9.5), respectively. Each of these events were characterized by rupture lengths of 750 and 1000 km, respectively, whereas our observations extend only ~ 400 km along the Indian HFT. The observations are consistent with the idea of simultaneous rupture of the sites in a single great earthquake.

An estimate of the time required to accumulate sufficient slip to produce similar size displacements to those we observe is obtained by dividing the vertical separation due to estimated single event displacements by the vertical uplift rates obtained from the uplifted terraces. To do so, we divide the vertical separation measurements of 7.5, 9.0, and 13.0 m obtained for Rampur Ganda, Lal Dhang and Ramnagar by the long term uplift rate of ≥ 4.8 $+ 0.9$ mm/yr, $\geq 6.9 \pm 1.8$ mm/yr, and 6.6-8.8 mm/yr obtained from uplifted terraces of the Markanda, Shahjahanpur, and Kosi Rivers. The exercise yields estimates of $\leq 1619 \pm 304$ years, $\leq 1417 \pm 383$ years and, $\leq 1723 \pm 246$ years for sufficient slip to accumulate to produce the observed coseismic slips, respectively. The result implies relatively long return times for such displacements within the central seismic gap.

Mechanics of rupture

Instrumentally recorded seismicity of moderate magnitude seismic events is concentrated beneath the High Himalaya (Ni and Barazangi, 1984), and geodetic monitoring also shows that interseismic elastic strain is presently accumulating beneath the High Himalaya (Bilham et al., 1997a; Jackson and Bilham, 1994; Pandey et al., 1995; Banerjee

and Burgmann, 2002). When combined with evidence of an emergent HFT, these observations are consistent with the interpretation that the major historical earthquakes initiated at a point of localized strain accumulation beneath the MCT and propagates southward as much as 100 km along a shallow décollement that surfaces as the HFT (Pandey et al., 1995; Brune, 1996; Bilham et al., 1998; Lave and Avouac, 2000).

The major plate boundary earthquakes that occurred in historical times along the HFT apparently have not produced coseismic surface ruptures. Given our observations showing evidence of surface rupturing earthquakes, the question arises why surface rupture has not been recorded during the major historical events. It seems unlikely but possible that studies of these major historical earthquakes missed evidence of surface rupture. If the historical earthquakes did not rupture the surface, how are we to interpret the surface ruptures that we do observe? Do the observations recorded in the trenches reflect events that initiate at the MCT and are large enough to propagate to the surface at the HFT and, therefore, yet larger than the major historical earthquakes that have been recorded? Or, do observations from Panchkula, Kala Amb, Dhanura, Dehra Dun, and Lal Dhang suggest that the earthquakes recorded in the trenches may represent lesser, though certainly large, displacements localized on the toe of an essentially flat and very shallow décollement surface of the HFT (e.g. Hino et al., 2000)? Alternatively, is it possible that none of the major historical earthquakes occurred on the HFT, as suggested recently for the 1897 earthquake of Assam (Bilham and England, 2001)? Given that our observations indicate coseismic displacement on the order of 15 to 25 m and the apparent synchronicity of events at sites spread ~400 km along the HFT (**Figure 19**), we suggest that the first possibility is the most likely that the

earthquake displacements we observe are the result of earthquakes larger than observed historically, and possibly the result of a rupture extending all or a major portion of the Indian HFT.

ACKNOWLEDGEMENTS

We thank Dr. Usha Malik (Principal) of Government College, Panchkula, and Mr. Dhanpat Singh, Higher Education Commissioner, Government of Haryana for granting permission to carry out trenching inside the premise of Government College, Panchkula. We also thank forest officials of Uttranchal Government, Mr. K.L. Arya, Mr. Jairaj, and Mr. Sinha for providing us permission to place trenches and sample pits in the Reserved and National Forest area of Uttranchal region. We thank Mr. Sanjay Verma for driving and helping us in the field. This material is based upon work supported by National Science Foundation Grant No. EAR9972955. This is Center for Neotectonic Studies contribution **45**.

REFERENCES CITED:

- Ambraseys, N. and Bilham, R., 2000. A note on the Kangra Ms = 7.8 earthquake of 4 April 1905. *Current Science*, 79: 45-50.
- Armijo, A., Tapponnier, P., Mercier, J.L. and Tonglin, H., 1986. Quaternary extension in southern Tibet. *Journal of Geophysical Research*, 91: 13,803-13,872.
- Armijo, A., Tapponnier, P. and Tonglin, H., 1989. Late Cenozoic right-lateral strike-slip faulting in southern Tibet. *Journal of Geophysical Research*, 94: 2787-2838.
- Avouac, J.P. and Tapponnier, P., 1993. Kinematic model of active deformation in Central Asia. *Geophysical Research Letters*, 20(10): 895-898.
- Banerjee, P. and Burgmann, R., 2002. Convergence across the northwest Himalaya from GPS measurements. *Geophysical Research Letters*, 29(13): 31-34.
- Bilham, R., Bodin, P. and Jackson, M., 1995. Entertaining a great earthquake in Western Nepal: Historic inactivity and geodetic tests for the present state of strain. *Journal of Nepal Geological Society*, 11(1): 73-78.
- Bilham, R., Larson, K.M., Freymueller, J. and members, P.I., 1997. GPS measurements of present day convergence across the Nepal Himalaya. *Nature (London)*, 386 (6620): 61-64.
- Bilham, R., Blume, F., Bendick, R. and Gaur, V.K., 1998. Geodetic constraints on the translation and deformation of India, implications for future great Himalayan earthquakes. *Current Science*, 74: 213-229.

- Bilham, R., 2001. Slow tilt reversal of the Lesser Himalaya between 1862 and 1992 at 78 deg. E, and bounds to the southeast rupture of the 1905 Kangra earthquake. *Geophysical Journal International*, 144: 713-728.
- Bilham, R. and England, P., 2001. Plateau pop-up in the 1897 Assam earthquake. *Nature*, 410: 806.
- Bilham, R., Gaur, V.K. and Molnar, P., 2001. Himalayan Seismic Hazard. *Science*, 293: 1442-1444.
- Brown, L.D. et al., 1996. Bright Spots, Structure, and Magmatism in Southern Tibet from INDEPTH Seismic Reflection Profiling. *Science*, 274: 1688-1691.
- Brune, J.N., 1996. Particle motions in a physical model of shallow angle thrust faulting. *Proceedings of the Indian Academy of Sciences: Earth and Planetary Sciences*, 105: L197-L206.
- Chander, R., 1989. Southern limits of major earthquake ruptures along the Himalaya between 15 deg. E and 90 deg. E. *Tectonophysics*, 170: 115-123.
- Demets, C., Gordon, R., Argus, D. and Stein, S., 1994. Effect of recent revisions to the geomagnetic reversal time scale on estimates of current plate motions. *Geophysical Research Letters*, 21: 2191-2194.
- Gansser, A., 1964. *Geology of the Himalayas*. London, Wiley Interscience: 289p.
- Hino, R., Ito, S., Shiobara, H., Shimamura, H., Sato, T., Kanazawa, T., Kasahara, J., and Hasegawa, A., 2000. Aftershock distribution of the 1994 Sanriku-oki earthquake (M_w 7.7) revealed by ocean bottom seismographic observation. *Journal of Geophysical Research*, 105 (B9): 21697-21710.

- Hodges, K.V., 2000. Tectonics of the Himalaya and Southern Tibet. Geological Society of America Bulletin, 112(3): 324-350.
- (http://www.haryana-online.com/pinjore_gardens.htm)
- Jackson, M.E. and Bilham, R., 1994. 1991-1992 GPS measurements across the Nepal Himalaya. Geophysical Research Letters, 21(12): 1169-1172.
- Johnson, M.R.W., 2000. Shortening budgets and role of continental subduction during the India-Asia collision. Earth-Science Reviews, 59: 101-123.
- Karunakaran, C. and Ranga Rao, A., 1976. Status of exploration for hydrocarbons in the Himalayan region - Contributions to stratigraphy and structure, Himalayan Geology seminar, section III, Oil and Natural Gas resources. Geological Survey of India Misc. Publ., 41: 1-66.
- Khattri, K.N., 1987. Great earthquakes, seismicity gaps and potential for earthquake disaster along the Himalaya Plate Boundary. Tectonophysics, 138: 79-92.
- Kumar, S. et al., 2001. Earthquake Recurrence and Rupture Dynamics of Himalayan Frontal Thrust, India. Science, 294(14 December): 2328-2331.
- Lave, J. and Avouac, J.P., 2000. Active folding of fluvial terraces across the Siwaliks Hills, Himalayas of central Nepal. Journal of Geophysical Research, 105(B3): 5735-5770.
- Lyon-Caen, H. and Molnar, P., 1985. Gravity anomalies, flexure of the Indian Plate, and the structure, support and evolution of the Himalaya and Ganga basin. Tectonics, 4: 513-538.
- Molnar, P. and Pandey, M.R., 1989. Rupture zones of great earthquakes in the Himalaya region. Earth Planetary Science, 98: 61-70.

- Molnar, P. and Tapponnier, P., 1977. The collision between India and Eurasia. *Scientific American*, 236: 30-41.
- Nakata, T., 1972. Geomorphic history and crustal movements of the foothills of the Himalayas. *Science Report Tohoku University, 7th Series*, 22: 39-177.
- Nakata, T., 1989. Active faults of the Himalaya of India and Nepal. *Geological Society of America special Paper*, 232: 243-264.
- Nanda, A.C., 1979. Occurrence of the Pre-Pinjor beds in the vicinity of Chandigarh. *Neogene/Quaternary Boundary Field Conference, India, Proceedings* 1981: 113-116.
- Nelson, K.D., 1998. The Himalaya and Tibetan Plateau; a perspective from project INDEPTH. In: Anonymous (Editor), *Geological Society of America, 1998 annual meeting. Abstracts with Programs - Geological Society of America*. Geological Society of America (GSA), Boulder, CO, United States, pp. 244.
- Ni, J. and Barazangi, M., 1984. Seismotectonics of the Himalayan collision zone: Geometry of the underthrusting Indian plate beneath the Himalaya. *Journal of Geophysical Research*, 89: 1147-1163.
- Pandey, M.R. and Molnar, P., 1988. The distribution of intensity of the Bihar-Nepal earthquake of 15 January 1934 and bounds on the extent of the rupture zone. *Journal of Geological Society of Nepal*, 5: 22-44.
- Pandey, M.R., Tandukar, R.P., Avouac, J.P., Lave, J. and Massot, J.P., 1995. Interseismic strain accumulation on the Himalayan crustal ramp (Nepal). *Geophysical Research Letters*, 22(7): 751-754.
- Paul, J. et al., 2001. The motion and active deformation of India. *Geophysical Research Letters*, 28: 647-650.

- Powers, P.M., Lillie, R.J. and Yeats, R.S., 1998. Structure and shortening of the Kangra and Dehra Dun Reentrants, Sub-Himalaya, India. Geological Society of America Bulletin, 110: 1010-1027.
- Raiverman, V., Srivastava, A.K. and Prasad, D.N., 1993. On the Foothill Thrust of northwestern Himalaya. Journal of Himalayan Geology, 4: 237-256.
- Rao, Y.S.N., Rahman, A. and Rao, D.P., 1974. On the structure of the Siwalik range between rivers Yamuna and Ganga. Himalayan Geology, 4: 137-150.
- Rao, Y.S.N., Rahman, A.A. and Rao, D.P., 1973. Wrench-faulting and its relationship to the structure of the southern margin of the Sub-Himalayan belt around Ramnagar, Uttar Pradesh. Journal of the Geological Society of India, 14(3): 249-256.
- Rupke, N., 1974. Stratigraphic and structural evolution of the Kumaon Lesser Himalaya. Sedimentary Geology, 11(Special Issue): 81-265.
- Sahni, M.R. and Kahn, E., 1964. Stratigraphy, structure and correlation of the Upper Siwaliks east of Chandigarh. Journal of Paleontological Society of India, 4: 59-72.
- Seeber, L. and Armbruster, J., 1981. Great detachment earthquakes along the Himalayan Arc and long-term forecasting. In: D.W. Simpson and P.G. Richards (Editors), Earthquake prediction; an international review. Maurice Ewing Series. American Geophysical Union, Washington, DC, United States, pp. 259-277.
- Seeber, L. and Gornitz, V., 1983. River profiles along the Himalayan arc as indicators of active tectonics. Tectonophysics, 92: 335-367.
- Srivastava, J.P., Verma, S.N., Joshi, V.K., Verma, B.C. and Arora, R.K., 1981. Review of some of the recent biostratigraphic work on the Siwalik rocks of Northwest Himalaya for Neogene-Quaternary Boundary and for the establishment of the Saketi

Fossil Park. GSI Proceedings, Neogene/Quaternary Boundary Field Conference, India, 1979.

Stein, R.S. and Yeats, R.S., 1989. Hidden Earthquakes. *Scientific American*, 260: 48-57.

Stuiver, M. and Polach, H.A., 1977. Discussion; reporting of C-14 data. *Radiocarbon*, 19 (3): 355-363.

Stuiver, M., and Reimer, P.J., 1993. Extended (super 14) C data base and revised CALIB 3.0 (super 14) C age calibration program. *Radiocarbon*, 35 (1): 215-230.

Stuiver, M., Reimer, P.J., Edouard, B., Beck, W.J., Burr, G. S., Hughen, K.A., Kromer, B., McCormac, G., van der Plicht, J., and Spurk, M., 1998. INTCAL98 radiocarbon age calibration, 24,000-0 cal BP. *Radiocarbon*, 40 (3): 1041-1083.

Thakur, V.C., 1995. Geology of Dun Valley, Garhwal Himalaya, neotectonics and coeval deposition with fault-propagation folds. *Journal of Himalayan Geology*, 6: 1-8.

Thakur, V.C. and Kumar, S., 1995. Seismotectonics of the 20 October 1991 Uttarkashi earthquake in Garhwal Himalaya, North India. In: H.K. Gupta and G.D. Gupta (Editors), *Uttarkashi earthquake (20th October 1991)*. Memoir - Geological Society of India. Geological Society of India, Bangalore, India, pp. 101-108.

Valdiya, K.S., 1992. The Main Boundary Thrust zone of the Himalaya, India. *Annales Tectonicase*, 6: 54-84.

Valdiya, K.S., 2003. Reactivation of Himalayan Frontal Fault: Implications. *Current Science*, vol. 85 (7): 1031 - 1040.

Wang, Q., Zhang, P., Freymueller, J.T., Bilham, R., Larson, K.M., Lai, X., You, X., Niu, Z., Wu, J., Li, Y., Liu, J., Yang, Z. and Chen, Q., 2001. Present-day crustal deformation

in China constrained by Global Positioning System Measurements, vol. 294: 574-577.

Wesnousky, S.G., Kumar, S., Mohindra, R. and Thakur, V.C., 1999. Uplift and convergence along the Himalayan Frontal Thrust of India. *Tectonics*, 18(6): 967-976.

Yeats, R.S. and Lillie, R.J., 1991. Contemporary tectonics of the Himalayan frontal fault system: Folds, blind thrusts and the 1905 Kangra earthquake. *Journal of Structural Geology*, 13: 215-225.

Yeats, R.S. et al., 1992. The Himalayan frontal fault system. *Annales Tectonicase*, 6 suppl.: 85-98.

Yeats, R.S. and Thakur, V.C., 1998. Reassessment of earthquake hazard based on a fault-bend fold model of the Himalayan plate-boundary fault. *Current Science*, 74: 230-233.

Zhao, W., Nelson, K.D., and project INDEPTH Team (1993). Deep seismic-reflection evidence continental underthrusting beneath southern Tibet. *Nature*, 366: 557-559.

FIGURE(S) CAPTION

Figure 1. (A) Major thrust faults and meizoseismal zones (shaded and labeled with date) of major historical earthquakes along the ~ 2500km long Himalayan arc. The extent of map area shown in Figure 2 is represented as bold polygon in Fig. 1A. Three major thrust faults are the Main Central Thrust (MCT), the Main Boundary Thrust (MBT) and Himalayan Frontal Thrust (HFT) (Nakata, 1972; 1989). All the thrust faults are inferred to root at depth in a mid-crustal ramp (MHT) (Zhao et al., 1993; Brown et al., 1996; Nelson, 1998). The arrow between the rupture bounds of 1905 Kangra earthquake and 1934 Bihar-Nepal earthquake is Central Seismic Gap of Khattri (1987). The inset shown on the right-hand corner of Figure 1A indicates that on-going convergence between the Indian and Eurasia is between 40 and 50 mm/year (Demets et al., 1994; Paul et al., 2001). (B) Generalized north-south geologic section across the Himalaya for the central portion of the Himalayan arc. Location of the cross section in map view is indicated by line connecting solid squares on Figure 1A (Seeber and Armbruster, 1981).

Figure 2. Geological map of the northwestern portion of the Himalaya (location shown in Figure 1), showing major tectonic features. Adapted from Karunakaran and Ranga Rao (1976); Powers et al. (1998), and from unpublished Oil and Natural Gas Commission (ONGC) maps. Box outlines portion of the Himalayan Frontal Thrust reviewed for this work along the strike of the Indian Sub-Himalaya. Dotted line shown in the map is inferred trace of the Himalayan Frontal Thrust (HFT), where scarps in Quaternary alluvium are distinct the fault is shown as bold line with teeth on hanging wall. Active fault traces are adapted after

Nakata (1972, 1989); Valdiya (1992); Wesnousky et al. (1999); Yeats and Lillie (1991); Yeats et al. (1992) and are also mapped during the fieldwork for the present study.

Figure 3. (left) Geology of Pinjore Dun area shows location of the Himalayan Frontal Thrust (HFT) (Nanda, 1979; Sahni and Kahn, 1964). The HFT within the study area outlined in the box is shown as bold lines where the thrust trace is distinct and as broken lines where thrust trace is inferred. Teeths are on the hanging wall. The mapped distribution of fluvial terrace deposits is shown as a bold box and corresponds to area of Figure 4. (right) Corona satellite image (outlined by dashed box at left) shows fluvial terrace deposits (lighter shade) along the Ghaggar River.

Figure 4. (left) Map shows fluvial terrace deposits distribution along the gorge portion of the Ghaggar River Terrace. The location of the trench is shown as long rectangle. Contours are at 20 m intervals. The military zone encompassed by bold dark line precluded detailed mapping of fluvial terraces that are preserved within the zone. Shown in the inset are the profile of terrace distributions and their relation to present river grade. (right) Photo at top shows the Lower River Terrace (LRT) preserved along southeastern bank of the Ghaggar River near the village of Gunthala. White open circle shows the radiocarbon sample location. View is towards east. Figure below shows typical character of strath terrace deposits of Lower River Terrace (LRT) resting unconformably over dipping beds of Siwaliks Group. Heavy black line shows the location of radiocarbon samples. Radiometric date of the charcoal sample reported in the figure is dendrochronologically corrected calendar age range in A.D.

Figure 5. Log of the sample pit wall showing stratigraphic units, description and radiocarbon sample locations with labels. The sample pit is located ~100 meters to the north of trench location in Figure 4 and is represented by solid square. Radiometric date of the charcoal sample reported in the figure is dendrochronologically corrected calendar age range in A.D.

Figure 6. Map of Chandigarh trench wall showing fault traces (F1, bold), amount of offset, stratigraphic units, description and radiocarbon sample locations. Outlined in the box is portion of the trench enlarged to show details of cross-cutting relationship between faulted Unit 7 and unfaulted Unit 8 (Figure 6B). Radiometric dates reported for the radiocarbon sample in the figure are dendrochronologically corrected calendar age ranges in B.C./A.D.

Figure 7. (left) Geology of the Kala Amb (SITE 2) and Rampur Ganda (SITE 3) areas (Srivastava et al., 1981). Shown in inset is the schematic cross-section that depicts structure as a fault-bend fold (modified from Kumar et al., 2001). Black Mango fault trace is shown in bold. Arrows on either side of the bold line indicate the sense of motion. The terrace distribution map area of Figure 8 is outlined as solid box. (center) Extent of corona satellite image outlined by dashed box at left. Fault trace (bold white line between arrows), town of Kala Amb (solid circle), and trench site annotated on satellite image. (right) Corona satellite image of the Rampur Ganda area showing trench location near outlet of western tributary of Somb Nadi (Nadi = River).

Figure 8. (top) Map of fluvial terrace deposits (black) along the Markanda River. Contours of 100m are solid and intervening 20m contours dashed. Inset shows typical character of

strath terrace deposit resting unconformably over dipping beds of Siwaliks Group. The strath deposits are typically composed of rounded pebble-cobble gravels capped by a fine-grained loamy sand unit. Map locations and context of dendrochronologically corrected ages of samples MT-001/5 and MT-001/3 is shown in map and inset, respectively. Heavy black line shows the location of radiocarbon samples in map view and in exposure section (modified from Kumar et al., 2001). (bottom) Photo of the Markanda River terrace and seen in the background is the steeply dipping Siwalik bedrock. View is to the southeast.

Figure 9. (top) Map of Rampur Ganda eastern trench wall showing fault traces (F1, F2, and F3 as bold lines), amount of offset, stratigraphic units, description and radiocarbon sample location with labels. Radiometric dates reported for the radiocarbon sample in the figure are dendrochronologically corrected calendar age ranges in B.C./A.D. (center) Detail of a portion of the trench log. (bottom) Scarp profile across the fault trace (actual trench log is shown as gray shaded polygon in the scarp profile).

Figure 10. (top) Geology of Dehra Dun modified from Thakur (1995) and Wesnousky et al. (1999). The terrace distribution map area of Figure 11 is outlined as a box in the figure (Wesnousky et al., 1999). (bottom) Extent of corona satellite image of the study area outlined by box at top. The fault is shown as solid line where distinct and dotted line where inferred.

Figure 11. The terrace distribution map along the Siwalik range front from near the Yamuna River in the west to the town of Mohand in the east (adapted and modified from Wesnousky et al., 1999). The distinct trace of the Himalayan Frontal Thrust (HFT) is

shown as a solid line with teeth on the hanging wall and as a dotted line where inferred. Circle and circle with cross are locations of Mohand deep well and nearby shallow exploratory well, respectively. Contours are at 100 m intervals within the bedrock Siwaliks and at 20 m intervals on the alluvial fans. Forest road that runs along the HFT is shown as double lines with hatch. The trench location map of Figure 12 is highlighted as rectangular box.

Figure 12. (top) Map of fluvial terrace deposits distribution along Khajnawara rao showing the location of the trench and strike of the HFT exposed (bold lines). Higher and lower fluvial terrace deposits are shown as shades of dark and light gray, respectively. Contours are at 20 m intervals. Forest road is shown in dotted lines. Solid circle represents the location of trenches. (bottom) Trench log of Khajnawara Rao showing fault trace (F1) in bold line. The units are labeled in numerically increasing order assigning the least for the oldest deposit and the key description of the units are presented in the text. Squiggly lines indicate shearing of the bedrock Siwalik and underlying Quaternary gravel deposits near the fault trace (F1).

Figure 13. (left) Geology of Lal Dhang area. Fault trace (bold), village of Lal Dhang (solid square) and location of trench site (fault trace dashed where approximate). (right) Extent of corona satellite image outlined by box at left.

Figure 14. (top) Illustration of Lal Dhang trench wall showing fault trace (F1), stratigraphic units and radiocarbon sample locations. (center) Photo mosaic of the trench log shown at

top. (bottom) Scarp profile across the fault trace (actual trench log is shown as gray shaded polygon in the scarp profile).

Figure 15. (left) Geology of Ramnagar area shows location of the Himalayan Frontal Thrust (HFT), bedrock geology, structural data and Quaternary river terraces (T) (Rao et al., 1973). The HFT within the study area is shown as bold lines where thrust trace is distinct and as broken lines where thrust trace is inferred. Teeths are on the hanging wall direction. (right) The CORONA satellite image of the study area shows fault trace, outline of fluvial terraces of the Kosi River (HRT = Higher River Terrace; MRT = Middle River Terrace; and LRT is Lower River Terrace) and trench location.

Figure 16. (left) Map of fluvial terrace deposits along the Kosi River. Contours intervals are 50 feet. Fault trace (bold), trench location (rectangular box), and radiocarbon samples (solid circle) are annotated in the map (fault trace dashed where approximate). Shown in the inset are profile of the Kosi River terraces and their relation to active river grade. (right) Photo at top shows middle river terrace (Qt2) deposits sitting unconformably on top of the bedrock Siwaliks. The dashed line indicates the contact between the fluvial terrace deposits and bedrock. In the middle is photo of sample pit (location of sample pit is shown as solid circle in the map at left). View is to the west. At bottom a schematic illustration of the sample pit which exposed the upper 2 meters of 15 m of strath terrace deposits. The exposed strath terrace deposits are typically composed of rounded cobble-boulder gravels capped by a fine-grained loamy sand unit. Map locations and context of dendrochronologically corrected ages of samples KMRT-03 and KMRT-07 is shown in map at left and sample pit log, respectively.

Figure 17. (top) Map of Ramnagar eastern trench wall showing fault traces (F1, F2, and F3 in bold), amount of offset, stratigraphic units, description and radiocarbon sample location with labels. Outlined in the boxes are portion of the trench zoomed in to show discrete offsets of individual fault strands. (bottom) Scarp profile across the fault trace (original trench log at top is shown as gray shaded region in profile).

Figure 18. (left) Map of fluvial terrace deposits along the Nandaur River. Contours intervals are at 100 m (left). Fault trace (bold), forest road (dashed double line), sample pit (soild square) are annotated in the map (trace dashed where approximate or eroded by Nandaur River). (right) Photo of the sample pit showing sample location in solid circle. The dashed white line represents the contact between upper pebble-cobble-boulder gravels and fine grained silty sand rich in pottery fragments.

Figure 19. Space-time diagram illustrates geological map of the northwestern portion of the Indian Himalaya (top), showing sites studied in boxes (adapted from Karunakaran and Ranga Rao (1976), Powers et al. (1998) and Unpublished Oil and Natural Gas Commission (ONGC) maps). Earthquake events interpreted in each of the trench sites is given with the age ranges in calendar years A.D. The coseismice slip (c.s.) and vertical separation (v.s.) of the corresponding earthquake is shown in meters. The height of each box is 2-sigma standard deviation of the C14 calendar age (bottom). A gray shaded region shows possible age range between 1404 A.D. and 1422 A.D. for the most recent event recorded in the trenches along ~400 km length of the Indian HFT . Solid bold line represents the extent of central seismic gap (>800 km) defined by Khattri (1987).

TABLE 1. RADIOCARBON ANALYSES OF DETRITAL CHARCOAL SAMPLES

Location	Sample no. and Laboratory no.*	$\delta^{13}\text{C}^{\ddagger}$	^{14}C age [†] ($\pm 1\sigma$), B.P.	Calendar age range [‡] in calendar Years B.C. and A.D. ($\pm 2\sigma$)
TRENCH – SITE 1				
Unit – 6	PAN-01 (97126)	-25.0	535 ± 35	1315 – 1354; 1387 – 1441 A.D.
Unit – 6	PAN-02 (94611)	-25.0	665 ± 40	1279 – 1330; 1341 – 1397 A.D.
Unit – 6	PAN-03 (94612)	-25.0	150 ± 40	1665 – 1784; 1790 – 1890; 1909 – 1950 A.D.
Unit – 5	PAN-05 (97127)	-25.0	1115 ± 35	783 – 789; 827 – 840; 863 – 1002; 1011 – 1016 A.D.
Unit – 5	PAN-08 (94613)	-25.0	2445 ± 50	762 – 678; 671 – 607; 601 – 404 B.C.
Unit – 5	PAN-09 (94614)	-25.0	230 ± 40	1522 – 1576; 1626 – 1689; 1729 – 1811; 1922 – 1949 A.D.
Unit – 6	PAN-11 (94615)	-25.0	310 ± 40	1482 – 1654 A.D.
Unit – 6	PAN-17 (94616)	-25.0	215 ± 35	1637 – 1688; 1729 – 1810; 1922 – 1949 A.D.
Unit – 5	PAN-23 (94617)	-25.0	595 ± 40	1299 – 1413 A.D.
Unit – 5	PAN-26 (94618)	-25.0	440 ± 50	1404 – 1523; 1564 – 1628 A.D.
Unit – 6	PAN-27 (94619)	-25.0	1250 ± 40	683 – 884 A.D.
TERRACE AND TERRACE PIT SAMPLES – SITE 1				
Terrace	JHA-02 (94620)	-25.0	-855 ± 45 (?)	post-1950
Terrace	GAG-05 (94622)	-25.0	735 ± 40	1216 – 1303; 1368 – 1383 A.D.
Terrace	GAG-03 (94621)	-25.0	645 ± 45	1284 – 1334; 1336 – 1401 A.D.
Pit	LRT-01 (97128)	-26.0	910 ± 25	1036 – 1191; 1201 – 1207 A.D.
TERRACE SAMPLES – SITE 2				
Terrace [¶]	MT001-5 (77316)	-25.0	4300 ± 40	3015 – 2878 B.C.
Terrace [¶]	MT001-3 (73705)	-28.4	4410 ± 40	3325 – 2915 B.C.
TRENCH – SITE 3				
Unit – 3	AB-08 (102806)	-25.0	530 ± 35	1319 – 1352; 1388 – 1442 A.D.
Unit – 2b'	AB-07 (102805)	-25.0	730 ± 35	1222 – 1301; 1371 – 1380 A.D.
Unit – 2b	AB-18 (102807)	-25.0	1500 ± 35	439 – 452; 463 – 518; 529 – 641 A.D.
TRENCH – SITE 5				
Unit – 3	LDT-02 (97120)	-24.6	865 ± 45	1039 – 1142; 1150 – 1261 A.D.
Unit – 4	LDT-11 (97121)	-24.2	660 ± 35	1282 – 1329; 1343 – 1395 A.D.
Unit – 3	LDT-15 (97122)	-24.4	840 ± 20	1163 – 1174; 1177 – 1257 A.D.
Unit – 6	LDT-31 (97123)	-25.2	375 ± 25	1445 – 1523; 1564 – 1628 A.D.
Unit – 7	LDT-32 (97124)	-23.7	410 ± 25	1436 – 1512; 1600 – 1614 A.D.
Unit – 6	LDT-43 (97125)	-25.0	470 ± 70	1306 – 1365; 1386 – 1527; 1554 – 1632 A.D.
TRENCH – SITE 6				
Unit – 5	BR-07 (102802)	-25.0	565 ± 45	1301 – 1371; 1380 – 1433 A.D.
Unit – 4	BR-06 (102801)	-25.0	695 ± 35	1263 – 1323; 1350 – 1390 A.D.
Unit – 3	BR-15 (102804)	-25.0	700 ± 35	1259 – 1322; 1350 – 1390 A.D.
Unit – 2	BR-09 (102803)	-25.0	990 ± 35	984 – 1069; 1080 – 1129; 1136 – 1158 A.D.
TERRACE PIT SAMPLES – SITE 6				
Pit	KMRT-03 (97129)	-26.1	4985 ± 25	3906 – 3900; 3894 – 3881; 3800 – 3701 B.C.
Pit	KMRT-07 (97130)	-28.8	6630 ± 25	5620 – 5567; 5565 – 5511; 5498 – 5485 B.C.
TERRACE SOIL PIT SAMPLES – SITE 7				
Soil Pit	NHRT-10 (97131)	-24.9	2335 ± 25	476 – 474; 446 – 444; 411 – 375; 370 – 364; 269 – 262 B.C.

* CAMS; Center for Accelerator Mass Spectrometry, Lawrence Livermore National Laboratory;

[†] $\delta^{13}\text{C}$ values are the assumed values according to Stuvier and Polach (1977) when given without decimal places. Values measured for the material itself are given with a single decimal place;

[‡] Reported ^{14}C ages use Libby's half-life of 5568 years;

[¶] Dendrochronologically calibrated age ranges were calculated with the University of Washington calibration program Calib 4.4, using the intercepts method (Stuiver et al., 1998; Stuiver and Reimer, 1993), and age ranges are often discontinuous.

[¶] Reported radiometric dates are obtained from Kumar et al. (2001).

TABLE 2: Shortening rates determined by various methods

Rate(mm/yr)	Method	Himalayan region	Author(s)	Time span
13 - 20	Retro deformation	Soan Syncline, Pakistan	Leathers, 1987; Johnson et al., 1986	Plio-Miocene
9 - 14	Retro deformation	Shortening between Soan Syncline & Salt Range Thrust, Pakistan	Baker et al., 1988	Plio-Miocene
22	Retro deformation	Shortening between Soan Syncline & MBT, Pakistan	Jaswal et al., 1997	Plio-Miocene
7	Retro deformation	Shortening between Domeli Anticline & Pabbi Hill, Pakistan	Pennock et al., 1989	Plio-Miocene
7-19	Retro deformation	Shortening between High- to Sub-Himalaya	Schelling, 1992; Schelling & Arita, 1991	Plio-Miocene
6 - 16	Retro deformation	Dehra Dun Re-entrant, India	Powers et al., 1998	Plio-Miocene
14 \pm 2	Retro deformation	Kangra Re-entrant, India	Powers et al., 1998	Plio-Miocene
18	Slip rate	Entire Himalayan arc	Avouac and Tapponnier, 1993	Plio-Miocene
18	Finite Element	Nepal, Assam	Peltzer and Saucier, 1996	Plio-Miocene
10	Finite Element	Jammu, India	Peltzer and Saucier, 1996	Plio-Miocene
15 \pm 5	Facies Migration (On lap)	Central/West, India	Lyon-Caen & Molnar, 1983 & 1985	Plio-Miocene
18 \pm 7	Facies Migration (On lap)	Central India	Molnar, 1987	Plio-Miocene
17	Seismicity, geodesy	Indian Himalayan arc	Molnar, 1990	~100 years
17.2	Seismicity, geodesy	Nepal	Bilham, 1997	Decadal
20 \pm 3	Seismicity, geodesy	Nepal	Bilham, 1998	Decadal
13.8 \pm 3.6	Offset Holocene terraces	Dehra Dun, Central, India	Wesnousky et al., 1999	Holocene
21 \pm 1.5	Offset late Pleistocene & Holocene terraces	Nepal	Lave and Avouac, 2000	Late Pleistocene & Holocene
4.8 - 15.7	Offset Holocene terraces	Kala Amb, Central/West, India	Kumar et al., 2001	Holocene
10.7 \pm 0.8	Offset Holocene terraces	Chandigarh, Western India	Present study	Holocene
6.6 - 8.8	Offset Holocene terraces	Ramnagar, Central India	Present study	Holocene
9.8 \pm 0.4	Offset Holocene terraces	Chor Gharia, Central India	Present study	Holocene

Data collected from Powers et al., 1998 and Johnson, 2002

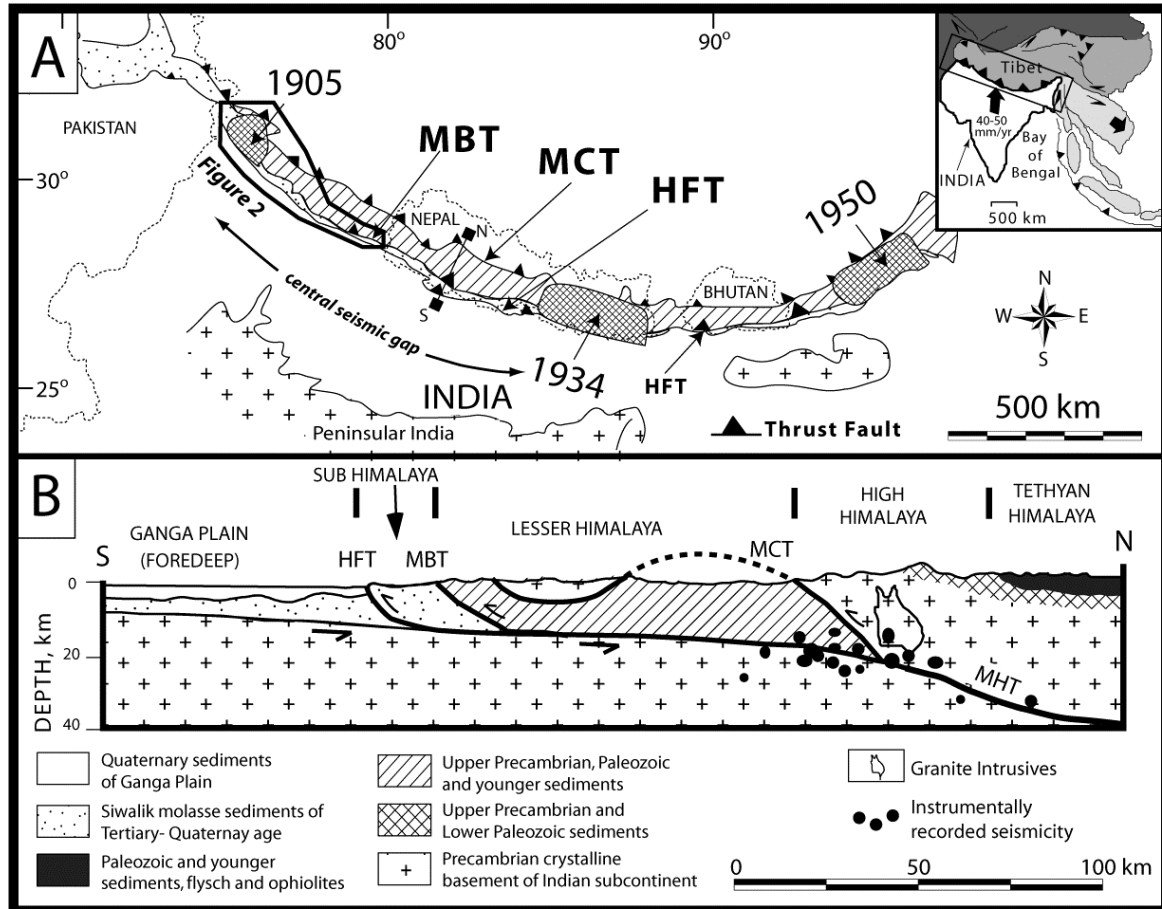


Figure 1. (A) Major thrust faults and meizoseismal zones (shaded and labeled with date) of major historical earthquakes along the ~ 2500km long Himalayan arc. The extent of map area shown in Figure 2 is represented as bold polygon in Fig. 1A. Three major thrust faults are the Main Central Thrust (MCT), the Main Boundary Thrust (MBT) and Himalayan Frontal Thrust (HFT) (Nakata, 1972; 1989). All the thrust faults are inferred to root at depth in a mid-crustal ramp (MHT) (Zhao et al., 1993; Brown et al., 1996; Nelson, 1998). The arrow between the rupture bounds of 1905 Kangra earthquake and 1934 Bihar-Nepal earthquake is Central Seismic Gap of Khattri (1987). The inset shown on the right-hand corner of Figure 1A indicates that on-going convergence between the Indian and Eurasia is between 40 and 50 mm/year (Demets et al., 1994; Paul et al., 2001). (B) Generalized north-south geologic section across the Himalaya for the central portion of the Himalayan arc. Location of the cross section in map view is indicated by line connecting solid squares on Figure 1A (Seeber and Armbruster, 1981).

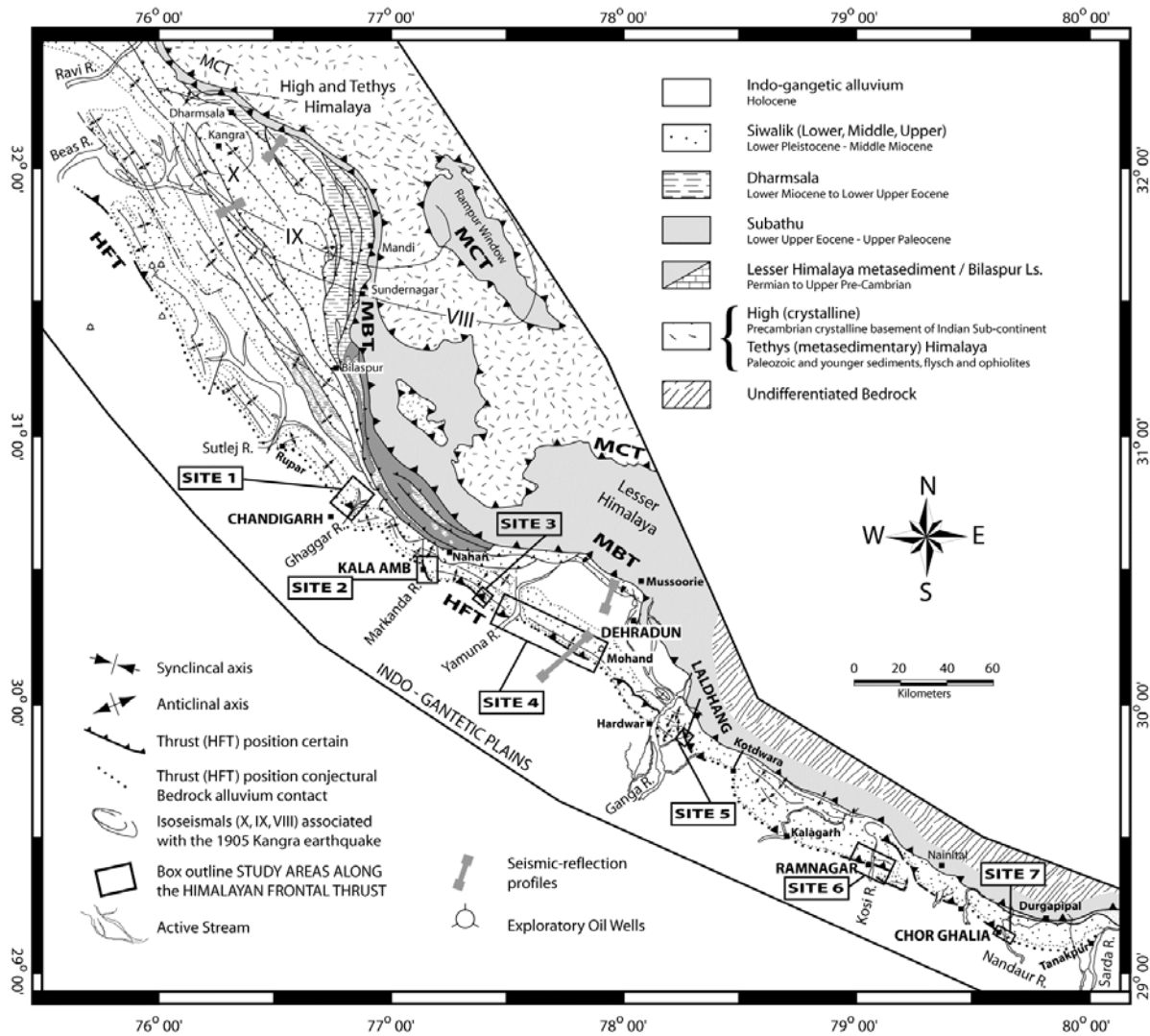


Figure 2. Geological map of the northwestern portion of the Himalaya (location shown in Figure 1), showing major tectonic features. Adapted from Karunakaran and Ranga Rao (1976); Powers et al. (1998), and from unpublished Oil and Natural Gas Commission (ONGC) maps. Box outlines portion of the Himalayan Frontal Thrust reviewed for this work along the strike of the Indian Sub-Himalaya. Dotted line shown in the map is inferred trace of the Himalayan Frontal Thrust (HFT), where scarps in Quaternary alluvium are distinct the fault is shown as bold line with teeth on hanging wall. Active fault traces are adapted after Nakata (1972, 1989); Valdiya (1992); Wesnousky et al. (1999); Yeats and Lillie (1991); Yeats et al. (1992) and are also mapped during the fieldwork for the present study.

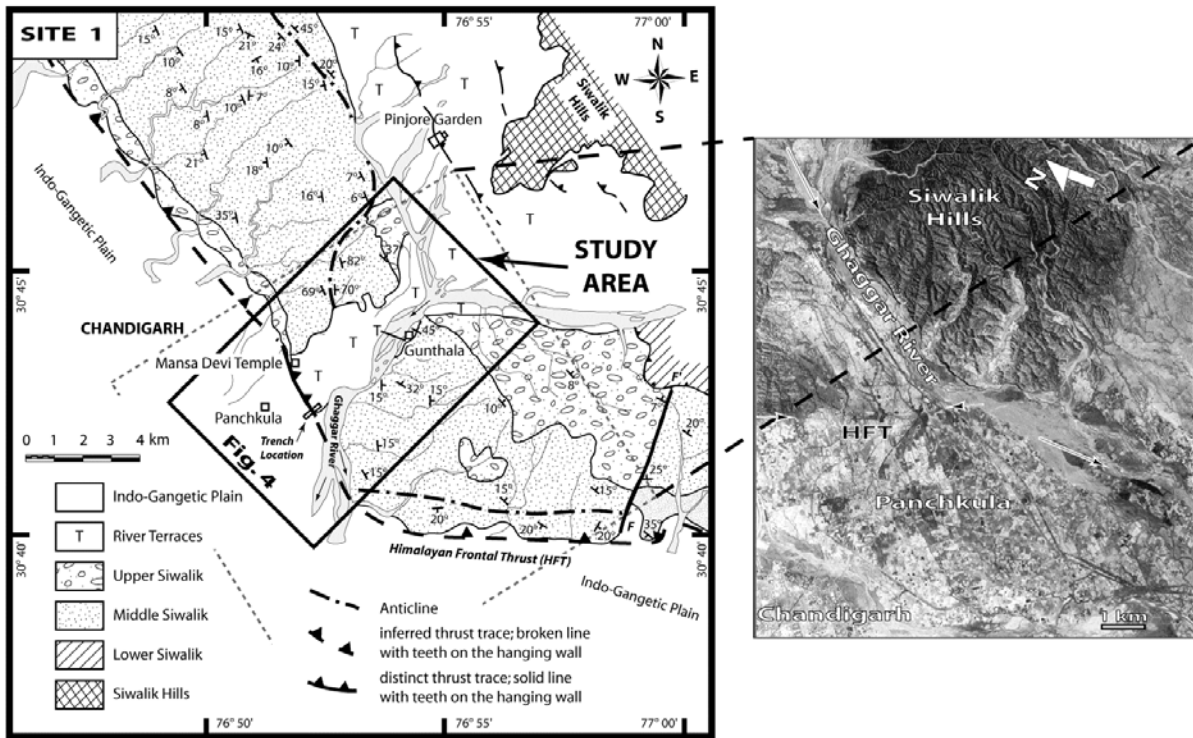


Figure 3. (left) Geology of Pinjore Dun area shows location of the Himalayan Frontal Thrust (HFT) (Nanda, 1979; Sahni and Kahn, 1964). The HFT within the study area outlined in the box is shown as bold lines where the thrust trace is distinct and as broken lines where thrust trace is inferred. Teeths are on the hanging wall. The mapped distribution of fluvial terrace deposits is shown as a bold box and corresponds to area of Figure 4. (right) Corona satellite image (outlined by dashed box at left) shows fluvial terrace deposits (lighter shade) along the Ghaggar River.

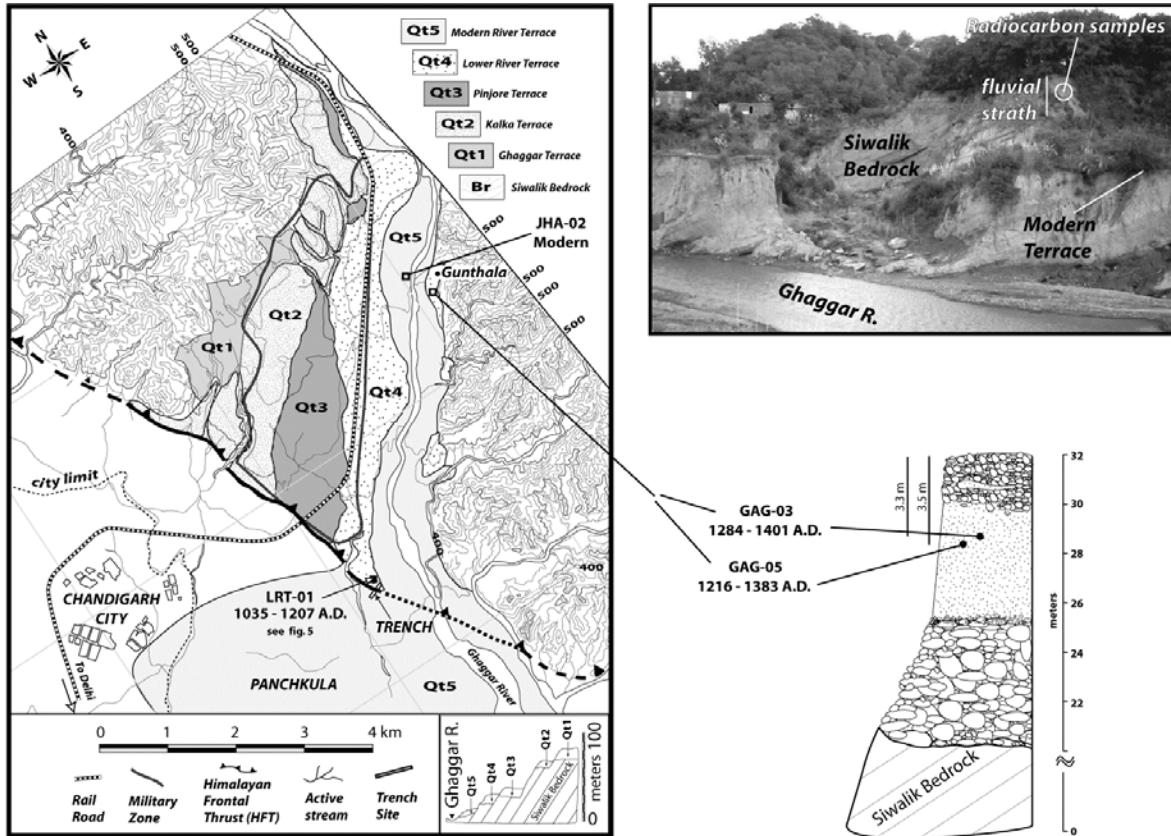


Figure 4. (left) Map shows fluvial terrace deposits distribution along the gorge portion of the Ghaggar River Terrace. The location of the trench is shown as long rectangle. Contours are at 20 m intervals. The military zone encompassed by bold dark line precluded detailed mapping of fluvial terraces that are preserved within the zone. Shown in the inset are the profile of terrace distributions and their relation to present river grade. (right) Photo at top shows the Lower River Terrace (LRT) preserved along southeastern bank of the Ghaggar River near the village of Gunthala. White open circle shows the radiocarbon sample location. View is towards east. Figure below shows typical character of strath terrace deposits of Lower River Terrace (LRT) resting unconformably over dipping beds of Siwaliks Group. Heavy black line shows the location of radiocarbon samples. Radiometric date of the charcoal sample reported in the figure is dendrochronologically corrected calendar age range in A.D.

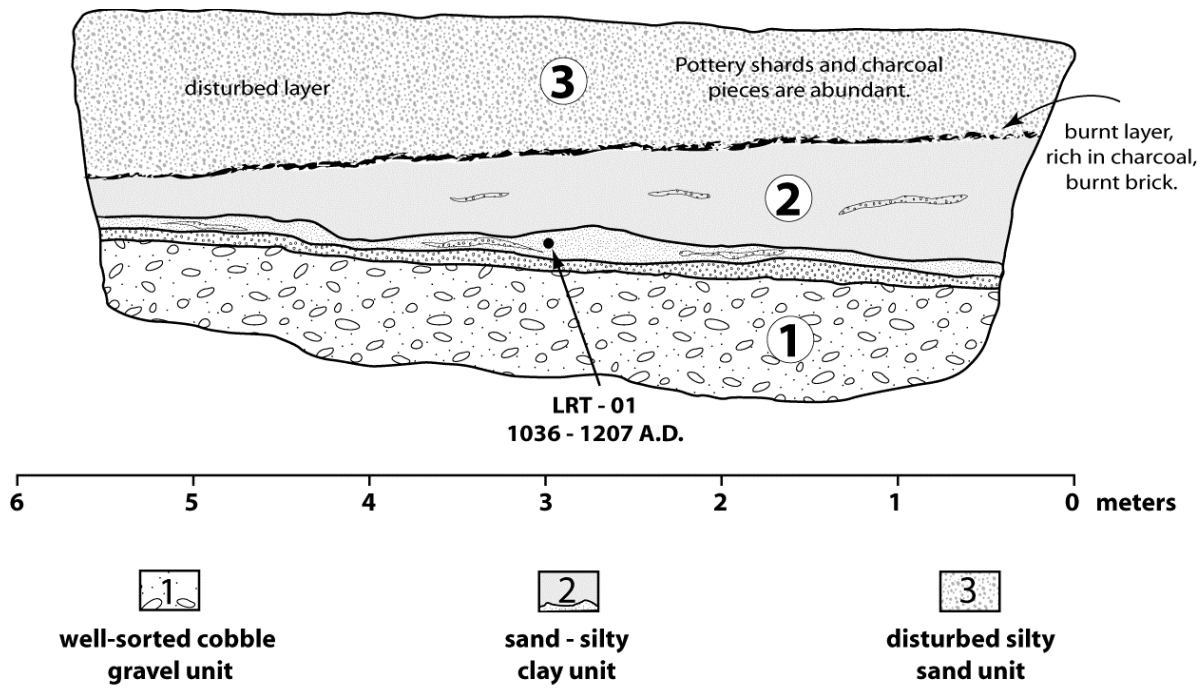


Figure 5. Log of the sample pit wall showing stratigraphic units, description and radiocarbon sample locations with labels. The sample pit is located ~100 meters to the north of trench location in Figure 4 and is represented by solid square. Radiometric date of the charcoal sample reported in the figure is dendrochronologically corrected calendar age range in A.D.

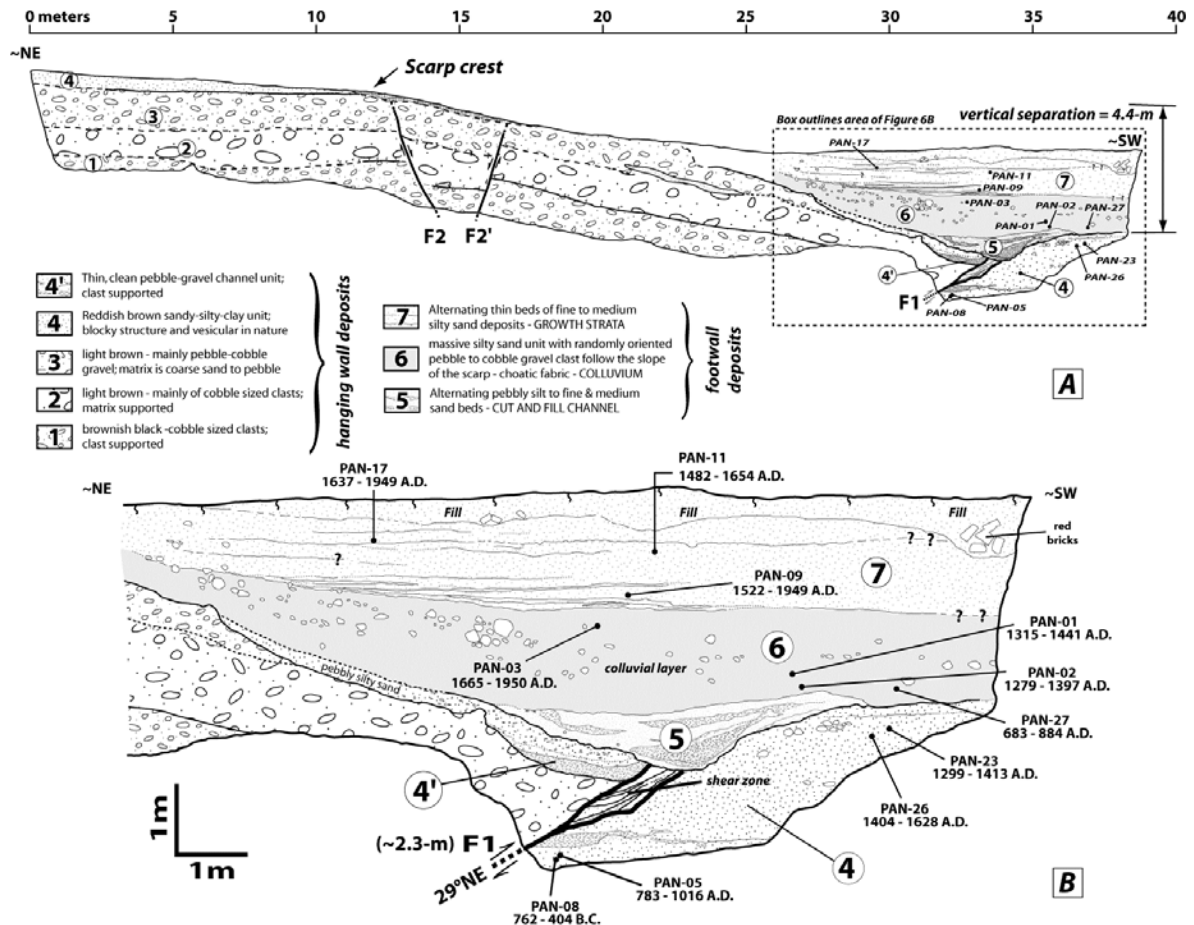


Figure 6. Map of Chandigarh trench wall showing fault traces (F1, bold), amount of offset, stratigraphic units, description and radiocarbon sample locations. Outlined in the box is portion of the trench enlarged to show details of cross-cutting relationship between faulted Unit 7 and unfaulted Unit 8 (Figure 6B). Radiometric dates reported for the radiocarbon sample in the figure are dendrochronologically corrected calendar age ranges in B.C./A.D.

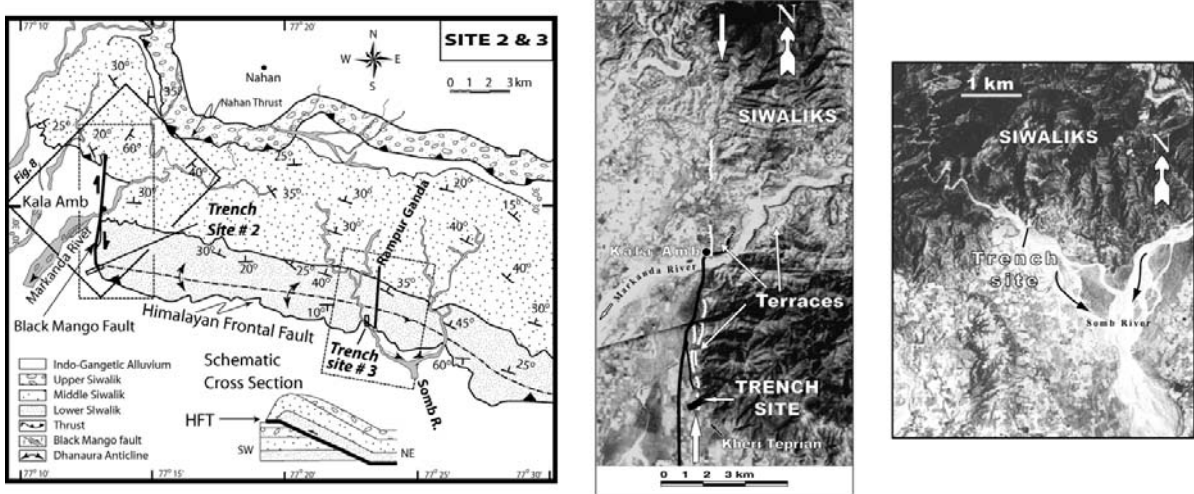


Figure 7. (left) Geology of the Kala Amb (SITE 2) and Rampur Ganda (SITE 3) areas (Srivastava et al., 1981). Shown in inset is the schematic cross-section that depicts structure as a fault-bend fold (modified from Kumar et al., 2001). Black Mango fault trace is shown in bold. Arrows on either side of the bold line indicate the sense of motion. The terrace distribution map area of Figure 8 is outlined as solid box. (center) Extent of corona satellite image outlined by dashed box at left. Fault trace (bold white line between arrows), town of Kala Amb (solid circle), and trench site annotated on satellite image. (right) Corona satellite image of the Rampur Ganda area showing trench location near outlet of western tributary of Somb Nadi (Nadi = River).

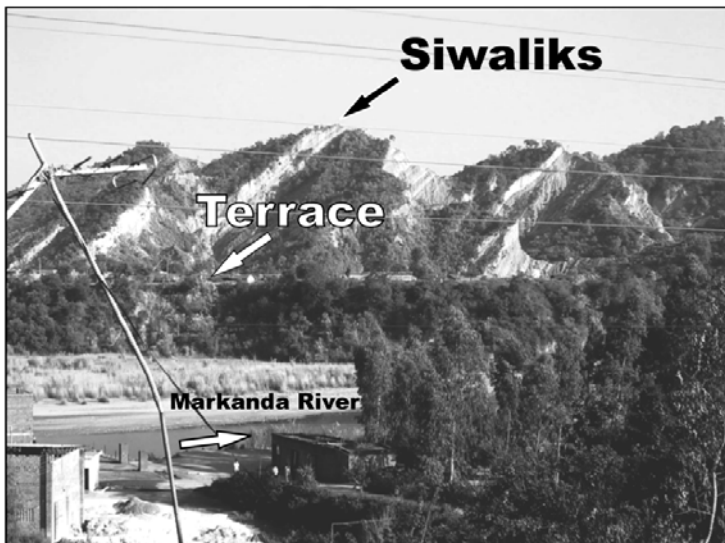
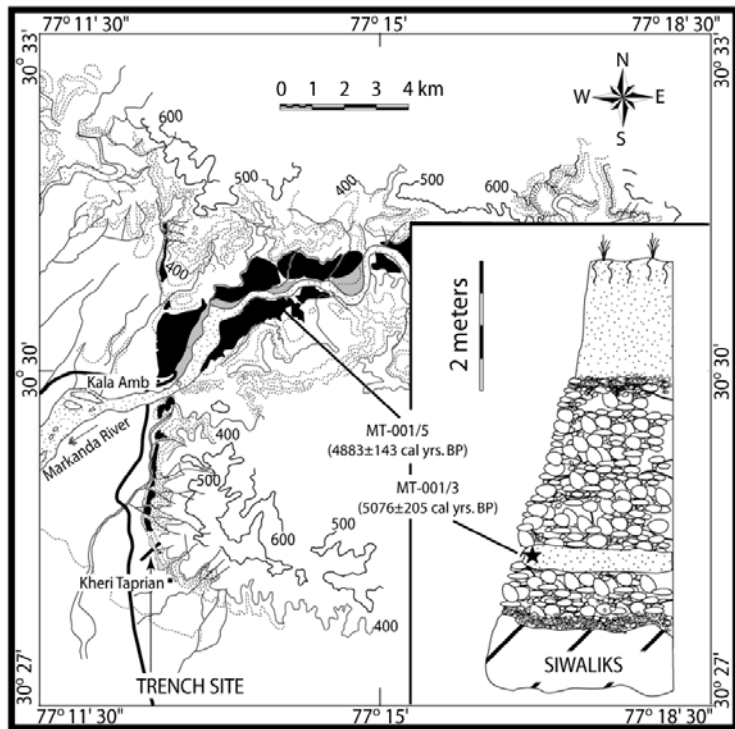


Figure 8. (top) Map of fluvial terrace deposits (black) along the Markanda River. Contours of 100m are solid and intervening 20m contours dashed. Inset shows typical character of strath terrace deposit resting unconformably over dipping beds of Siwaliks Group. The strath deposits are typically composed of rounded pebble-cobble gravels capped by a fine-grained loamy sand unit. Map locations and context of dendrochronologically corrected ages of samples MT-001/5 and MT-001/3 is shown in map and inset, respectively. Heavy black line shows the location of radiocarbon samples in map view and in exposure section (modified from Kumar et al., 2001). (bottom) Photo of the Markanda River terrace and seen in the background is the steeply dipping Siwalik bedrock. View is to the southeast.

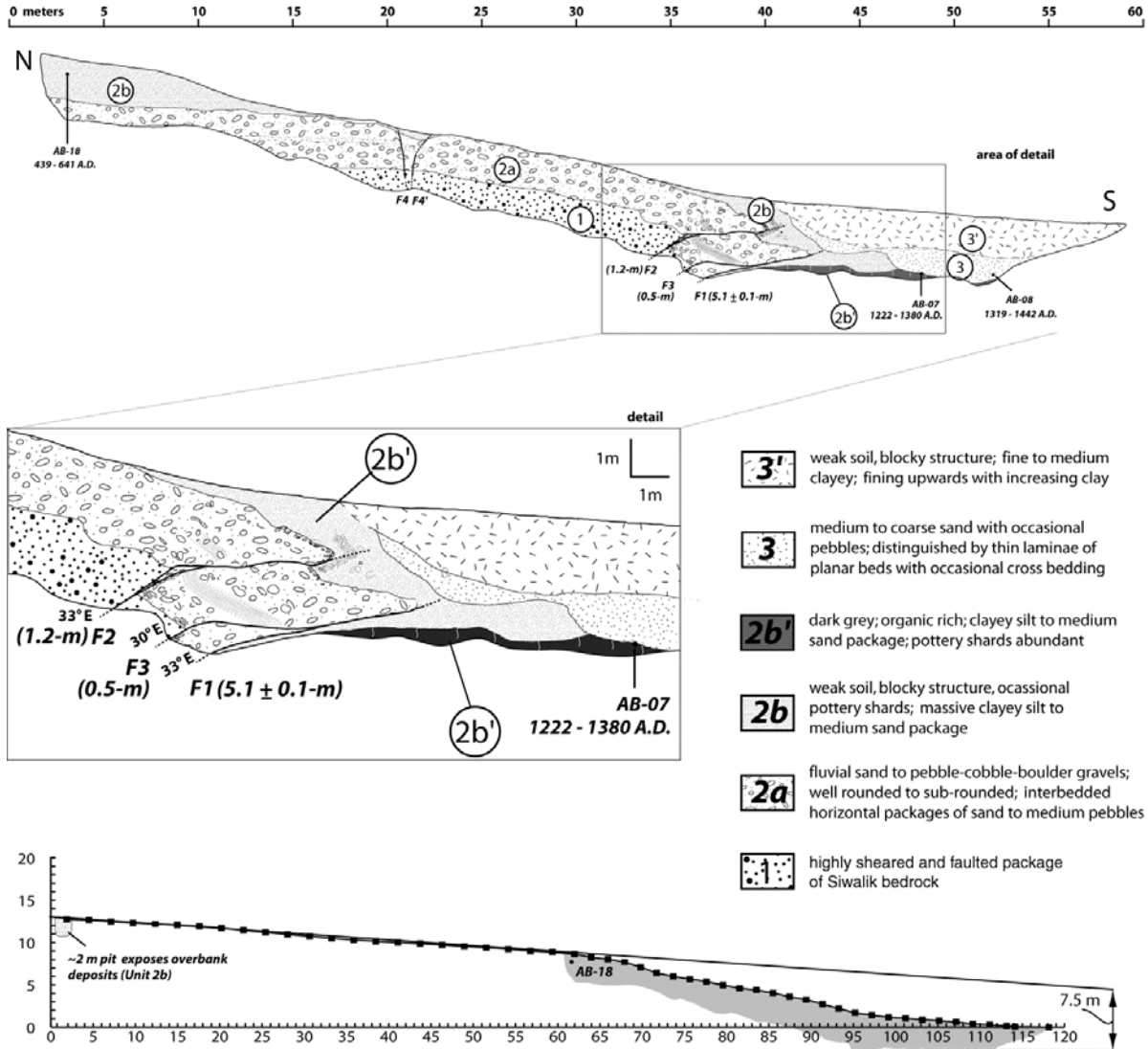


Figure 9. (top) Map of Rampur Ganda eastern trench wall showing fault traces (F1, F2, and F3 as bold lines), amount of offset, stratigraphic units, description and radiocarbon sample location with labels. Radiometric dates reported for the radiocarbon sample in the figure are dendrochronologically corrected calendar age ranges in B.C./A.D. (center) Detail of a portion of the trench log. (bottom) Scarp profile across the fault trace (actual trench log is shown as gray shaded polygon in the scarp profile).

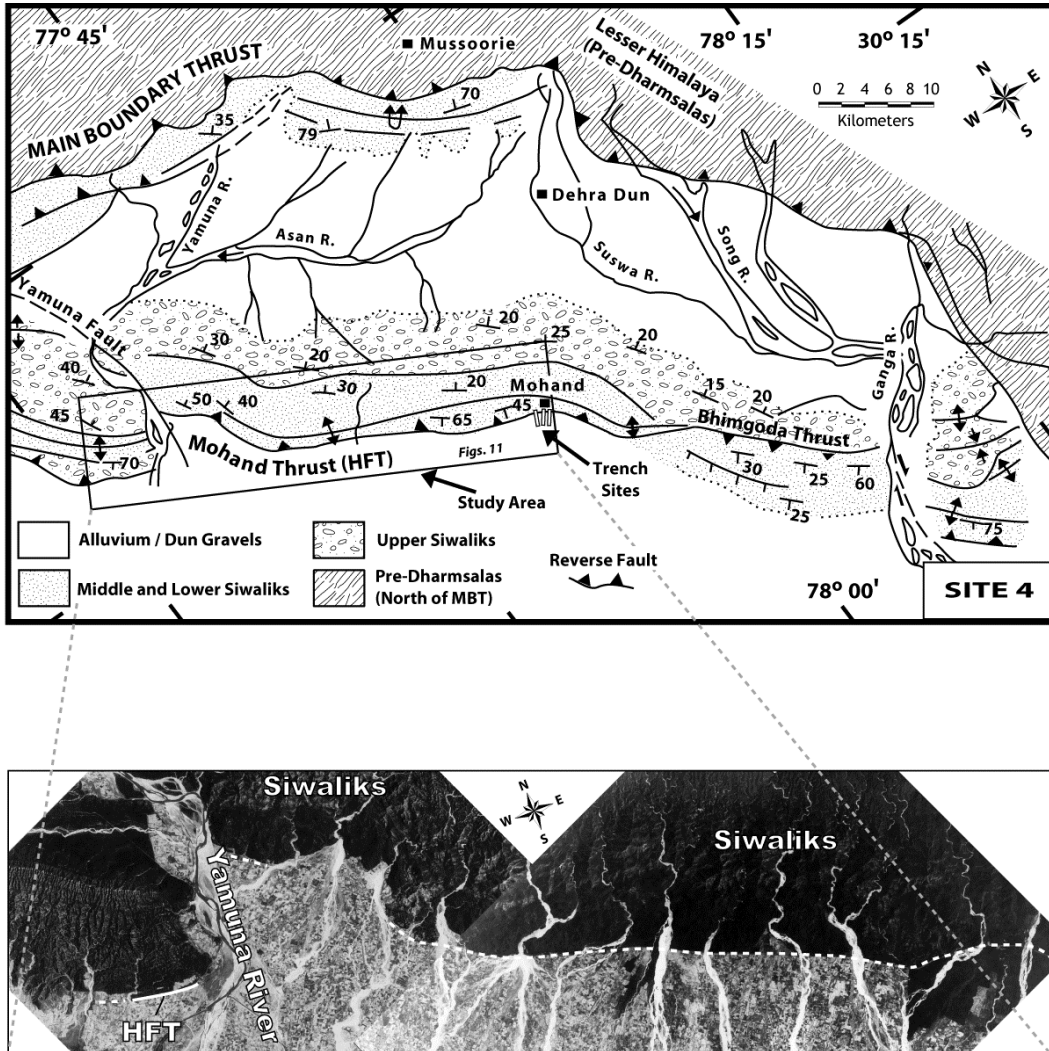


Figure 10. (top) Geology of Dehra Dun modified from Thakur (1995) and Wesnousky et al. (1999). The terrace distribution map area of Figure 11 is outlined as a box in the figure (Wesnousky et al., 1999). (bottom) Extent of corona satellite image of the study area outlined by box at top. The fault is shown as solid line where distinct and dotted line where inferred.

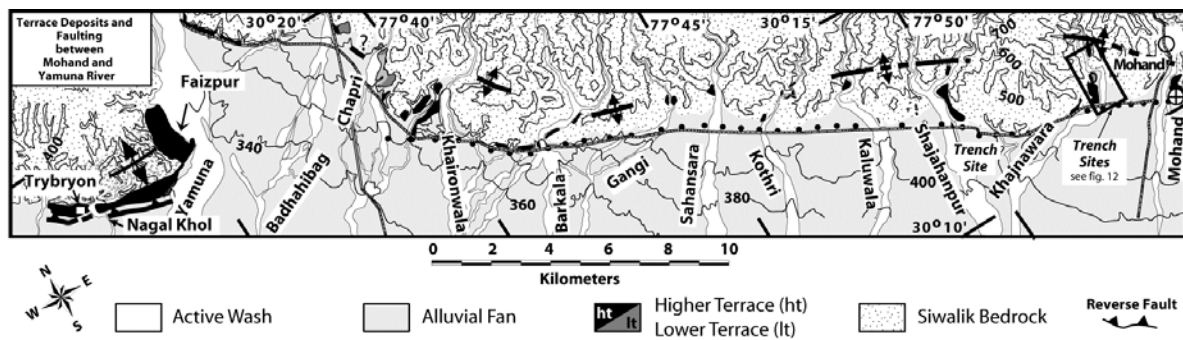


Figure 11. The terrace distribution map along the Siwalik range front from near the Yamuna River in the west to the town of Mohand in the east (adapted and modified from Wesnousky et al., 1999). The distinct trace of the Himalayan Frontal Thrust (HFT) is shown as a solid line with teeth on the hanging wall and as a dotted line where inferred. Circle and circle with cross are locations of Mohand deep well and nearby shallow exploratory well, respectively. Contours are at 100 m intervals within the bedrock Siwaliks and at 20 m intervals on the alluvial fans. Forest road that runs along the HFT is shown as double lines with hatch. The trench location map of Figure 12 is highlighted as rectangular box.

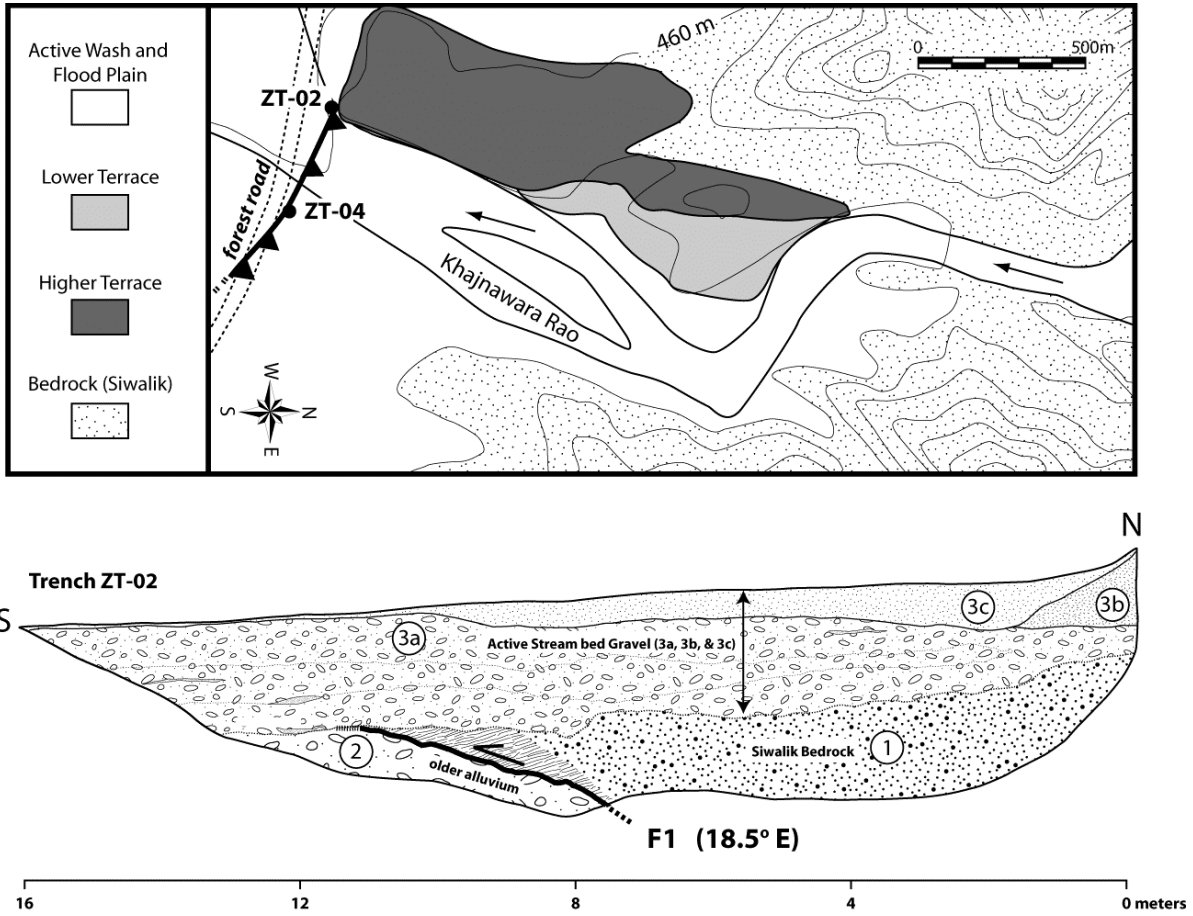


Figure 12. (top) Map of fluvial terrace deposits distribution along Khajnawara rao showing the location of the trench and strike of the HFT exposed (bold lines). Higher and lower fluvial terrace deposits are shown as shades of dark and light gray, respectively. Contours are at 20 m intervals. Forest road is shown in dotted lines. Solid circle represents the location of trenches. (bottom) Trench log of Khajnawara Rao showing fault trace (F1) in bold line. The units are labeled in numerically increasing order assigning the least for the oldest deposit and the key description of the units are presented in the text. Squiggly lines indicate shearing of the bedrock Siwalik and underlying Quaternary gravel deposits near the fault trace (F1).

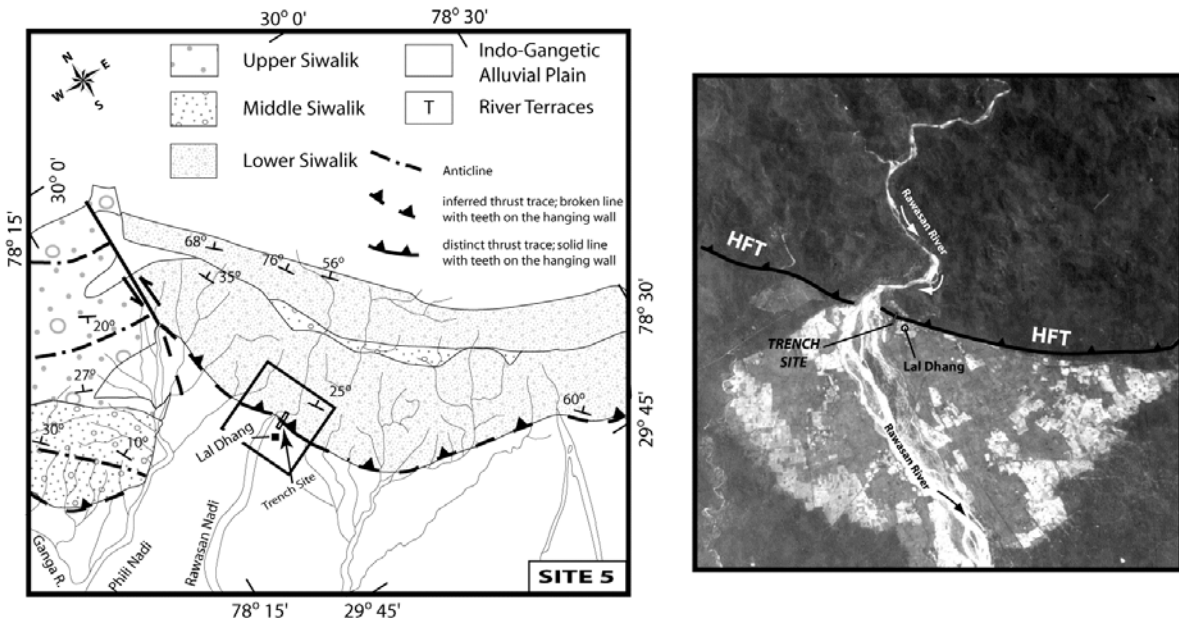


Figure 13. (left) Geology of Lal Dhang area. Fault trace (bold), village of Lal Dhang (solid square) and location of trench site (fault trace dashed where approximate). (right) Extent of corona satellite image outlined by box at left.

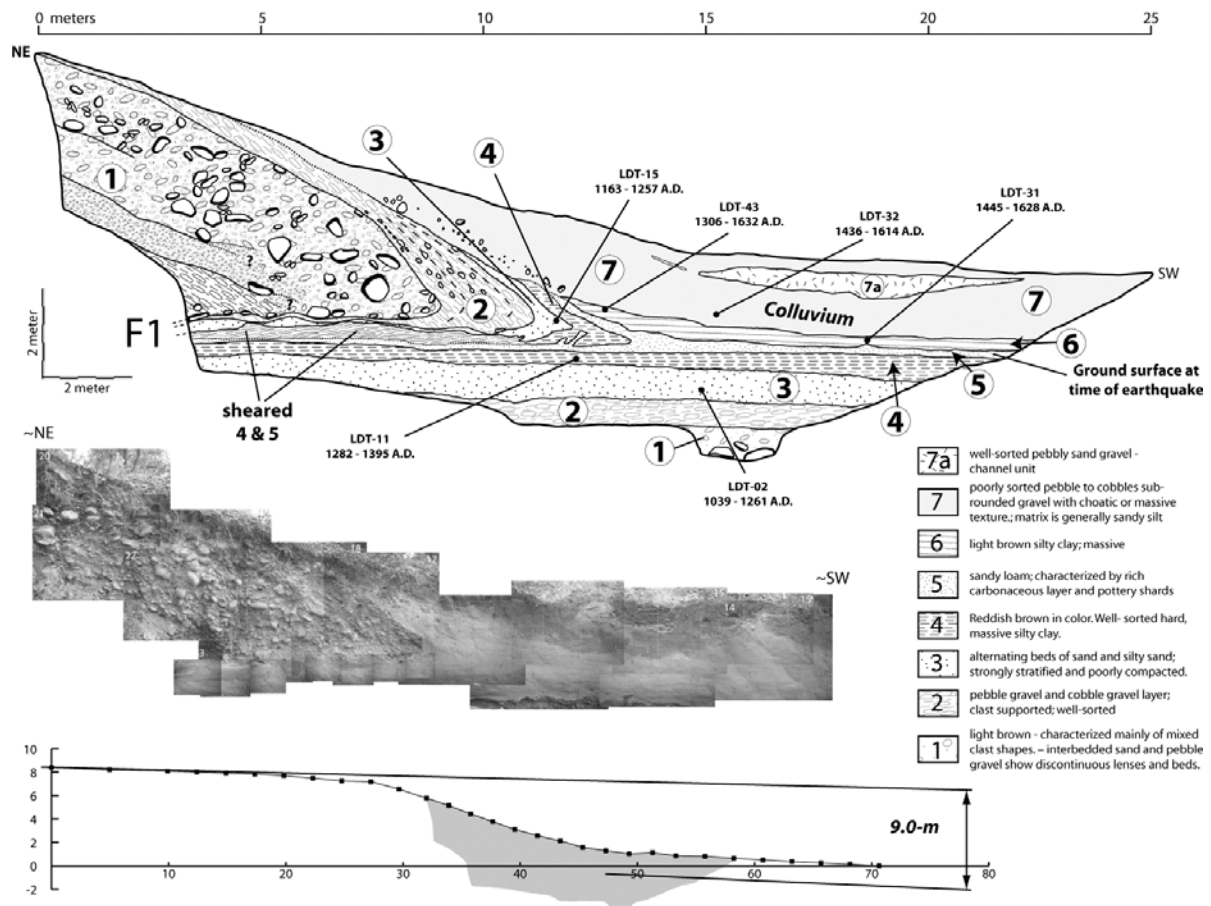


Figure 14. (top) Illustration of Lal Dhang trench wall showing fault trace (F1), stratigraphic units and radiocarbon sample locations. (center) Photo mosaic of the trench log shown at top. (bottom) Scarp profile across the fault trace (actual trench log is shown as gray shaded polygon in the scarp profile).

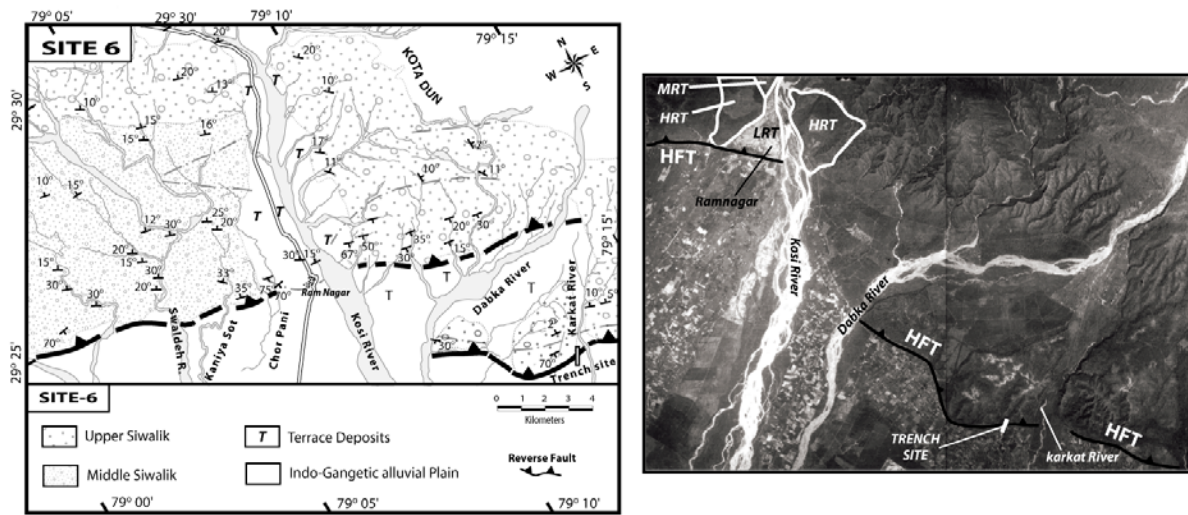


Figure 15. (left) Geology of Ramnagar area shows location of the Himalayan Frontal Thrust (HFT), bedrock geology, structural data and Quaternary river terraces (T) (Rao et al., 1973). The HFT within the study area is shown as bold lines where thrust trace is distinct and as broken lines where thrust trace is inferred. Teeths are on the hanging wall direction. (right) The CORONA satellite image of the study area shows fault trace, outline of fluvial terraces of the Kosi River (HRT = Higher River Terrace; MRT = Middle River Terrace; and LRT is Lower River Terrace) and trench location.

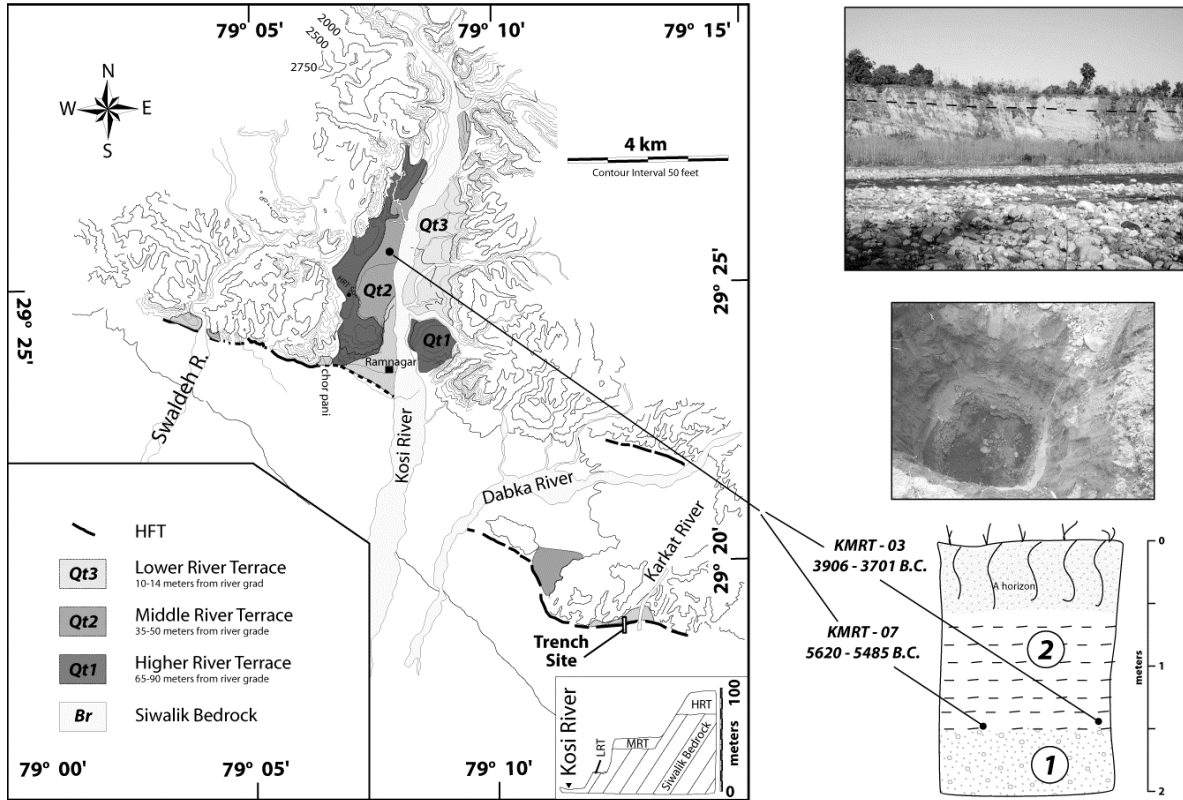


Figure 16. (left) Map of fluvial terrace deposits along the Kosi River. Contours intervals are 50 feet. Fault trace (bold), trench location (rectangular box), and radiocarbon samples (solid circle) are annotated in the map (fault trace dashed where approximate). Shown in the inset are profile of the Kosi River terraces and their relation to active river grade. (right) Photo at top shows middle river terrace (Qt2) deposits sitting unconformably on top of the bedrock Siwaliks. The dashed line indicates the contact between the fluvial terrace deposits and bedrock. In the middle is photo of sample pit (location of sample pit is shown as solid circle in the map at left). View is to the west. At bottom a schematic illustration of the sample pit which exposed the upper 2 meters of 15 m of strath terrace deposits. The exposed strath terrace deposits are typically composed of rounded cobble-boulder gravels capped by a fine-grained loamy sand unit. Map locations and context of dendrochronologically corrected ages of samples KMRT-03 and KMRT-07 is shown in map at left and sample pit log, respectively.

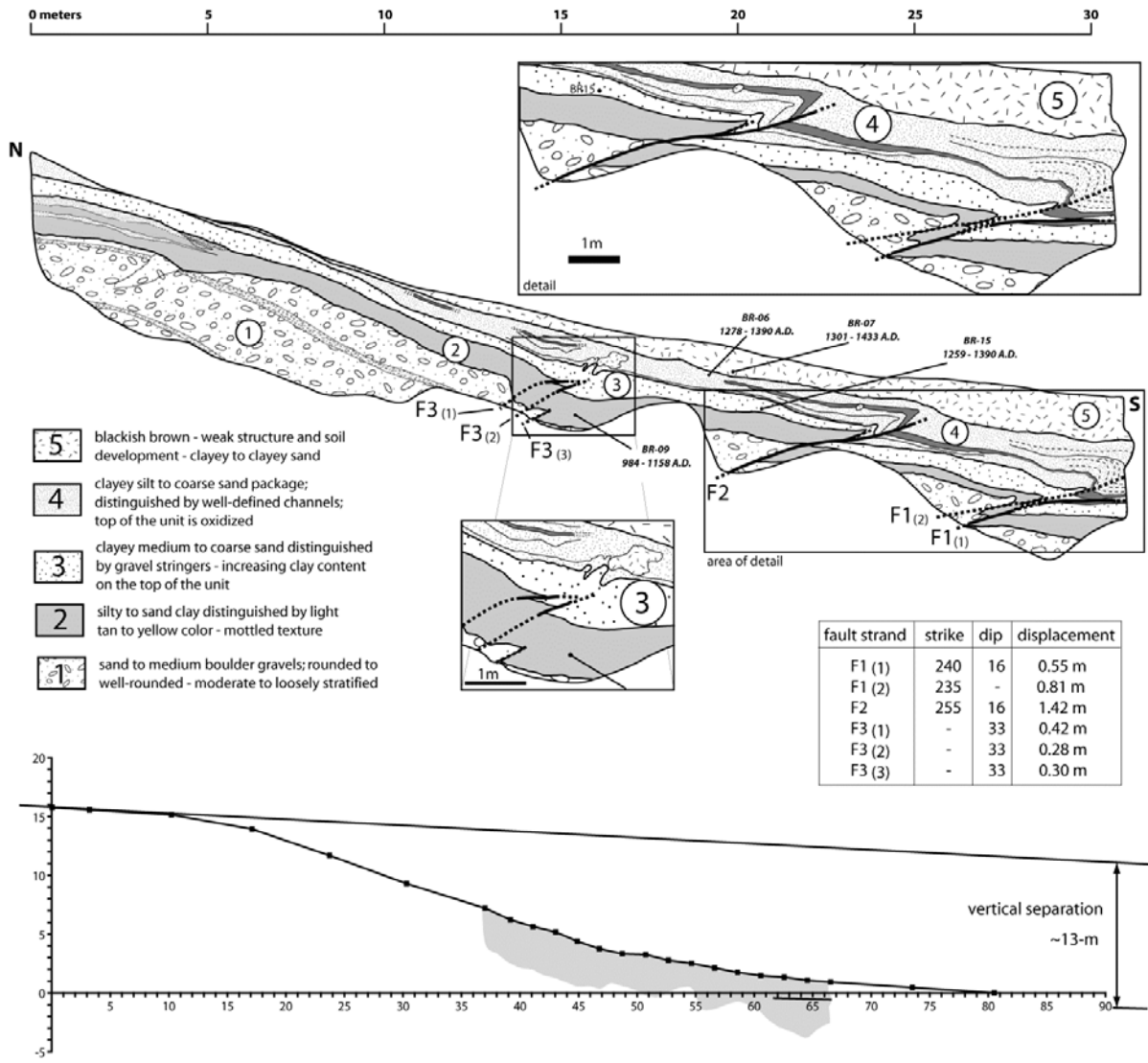


Figure 17. (top) Map of eastern trench wall showing fault traces (F1, F2, and F3 in bold), amount of offset, stratigraphic units, description and radiocarbon sample location with labels. Outlined in the boxes are portion of the trench zoomed in to show discrete offsets of individual fault strands. (bottom) Scarp profile across the fault trace (original trench log at top is shown as gray shaded region in profile).

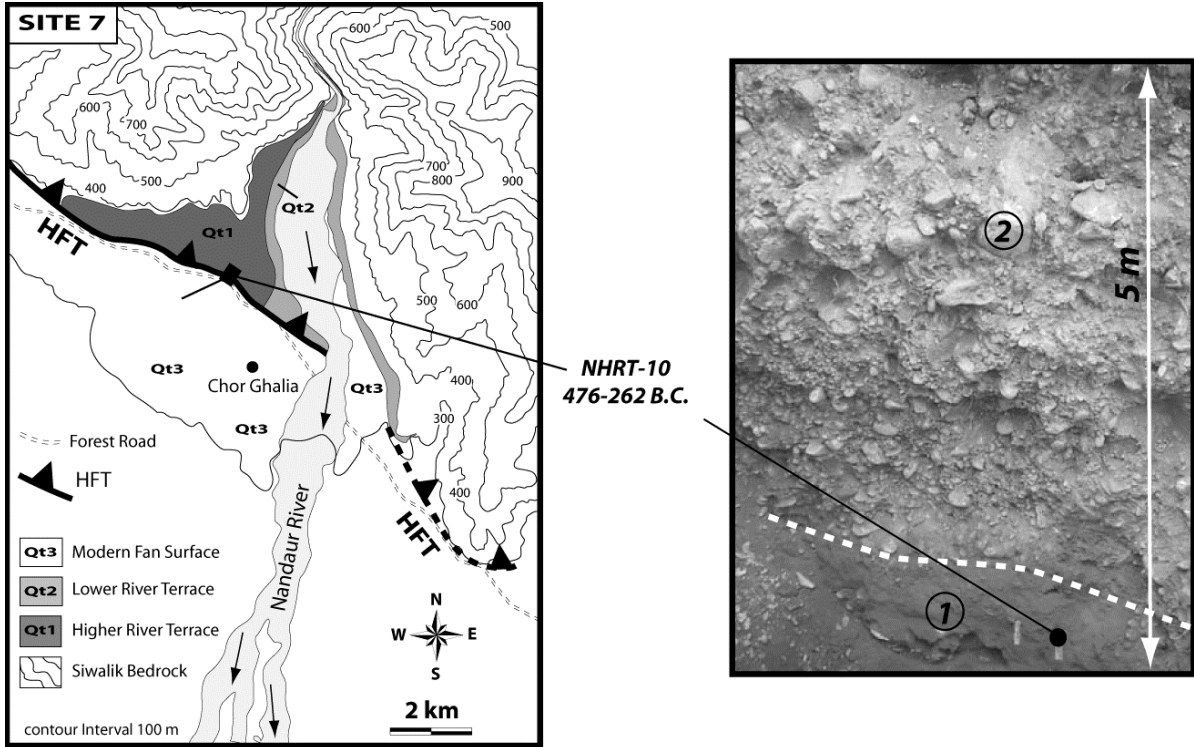


Figure 18. (left) Map of fluvial terrace deposits along the Nandaur River. Contours intervals are at 100 m (left). Fault trace (bold), forest road (dashed double line), sample pit (solid square) are annotated in the map (trace dashed where approximate or eroded by Nandaur River). (right) Photo of the sample pit showing sample location in solid circle. The dashed white line represents the contact between upper pebble-cobble-boulder gravels and fine grained silty sand rich in pottery fragments.

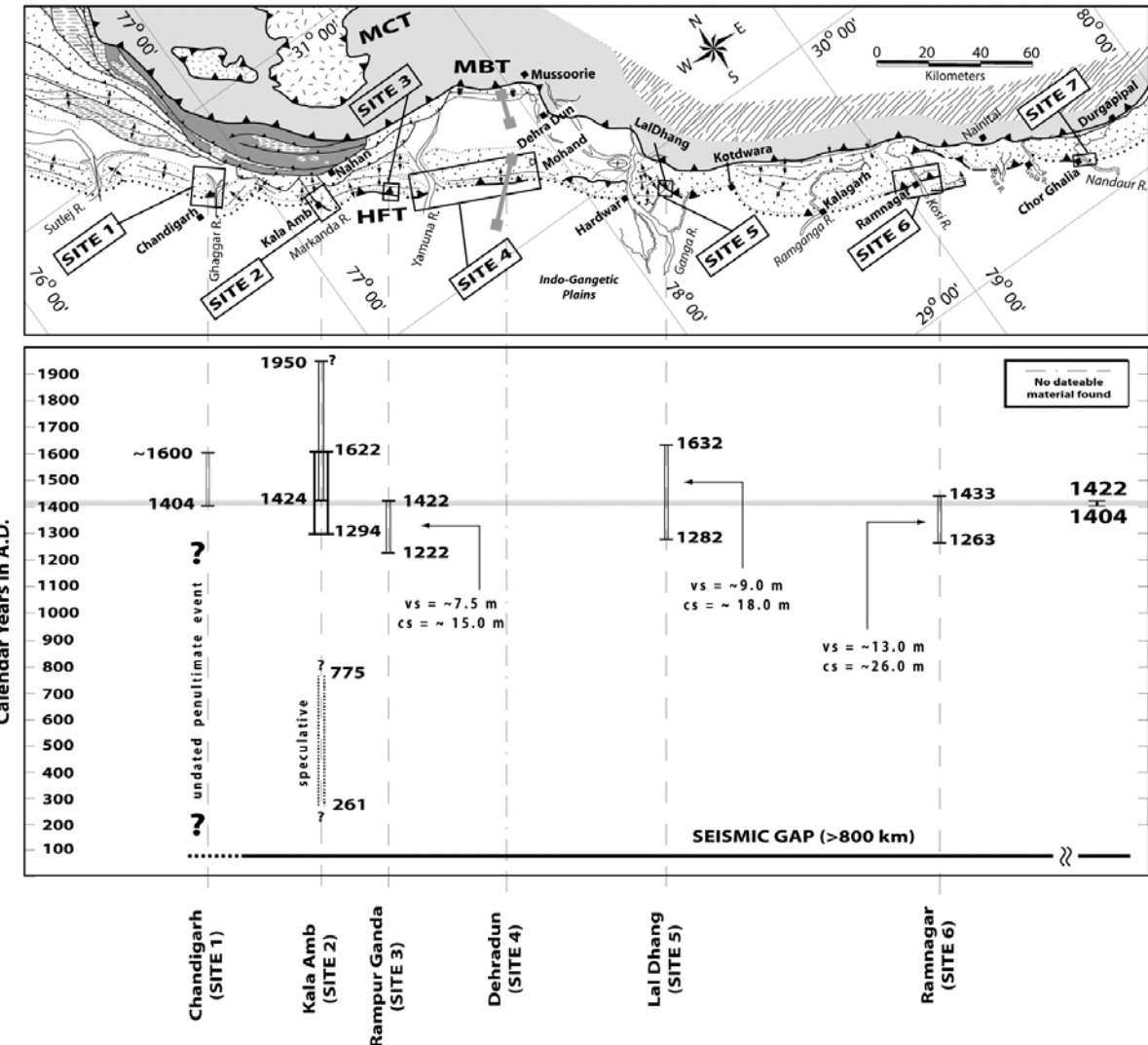


Figure 19. Space-time diagram illustrates geological map of the northwestern portion of the Indian Himalaya (top), showing sites studied in boxes (adapted from Karunakaran and Ranga Rao (1976), Powers et al. (1998) and Unpublished Oil and Natural Gas Commission (ONGC) maps). Earthquake events interpreted in each of the trench sites is given with the age ranges in calendar years A.D. The coseismice slip (c.s.) and vertical separation (v.s.) of the corresponding earthquake is shown in meters. The height of each box is 2-sigma standard deviation of the ^{14}C calendar age (bottom). A gray shaded region shows possible age range between 1404 A.D. and 1422 A.D. (or, 1413 + 9 A.D.) for the most recent event recorded in the trenches along ~400 km length of the Indian HFT . Solid bold line represents the extent of central seismic gap (>800 km) defined by Khattri (1987).